Mica-group minerals from carbonatites and related rocks: Paragenetic constraints, compositional variation and implications for carbonatite petrogenesis

Anton R. Chakhmouradian [a,*], Ekaterina P. Reguir [a], Anatoly N. Zaitsev [b,c], Cheng Xu [d], Yan Liu [e], Panseok Yang [a]

[a] Department of Geological Sciences, University of Manitoba, Winnipeg, Manitoba, Canada
[b] Department of Mineralogy, St. Petersburg State University, St. Petersburg, Russia
[c] Department of Earth Sciences, The Natural History Museum, London, UK
[d] Laboratory of Orogenic Belts and Crustal Evolution, Peking University, Beijing, China
[e] Chinese Academy of Geological Sciences, Beijing, China
* Corresponding author at: 125 Dysart Road, Department of Geological Sciences, University of Manitoba, Winnipeg, Manitoba R3T 2N2, Canada.
E-mail address: Anton.Chakhmouradian@umanitoba.ca (A.R. Chakhmouradian)

Introduction

Despite being a rather exotic rock type (~550 confirmed localities worldwide), carbonatites no longer need an introduction: the memorable, albeit short-lived rare-earth market crisis of 2010-2012 brought these rocks into the spotlight as one of the major sources of Nd and several other critical metals (Chakhmouradian and Wall, 2012; Chakhmouradian et al., 2015; Mitchell, 2015; Smith et al., 2016). Some 200 peer-reviewed papers on natural and synthetic carbonatite systems have been published in the past five years alone, including descriptions of at least 15 new occurrences. The distribution of carbonatites, their major structural and textural features, and relevant petrogenetic models have been discussed in a number of recent studies (Lee and Wyllie, 1998; Bell and Rukhlov, 2004; Mitchell, 2005; Woolley and Kjarsgaard, 2008; Chakhmouradian et al., 2016) and will not be repeated here.

As has been emphasized by several previous workers (Mitchell, 2005; Chakhmouradian et al., 2016; Mitchell and Smith, 2017), the formal definition of carbonatites endorsed by the International Union of Geological Sciences (Le Maitre, 2002) does not give due credit to the role of non-carbonate minerals in their modal composition, nor recognizes the diversity of silicate-carbonate (± oxide ± apatite) rocks that evidently originate from a carbonatitic source, but fail to meet the "official" criteria. Among these non-carbonate constituents, micas are undoubtedly the most important silicate minerals, because they: (1) are common in both calcite and dolomite carbonatites; (2) occur in intrusive and extrusive facies, as well as in contact-metasomatic rocks associated with carbonatites; and (3) have been reported in carbonatites from all major tectonic settings (rifts, orogenic belts and ocean islands). Micas are an important Rb-Sr and Ar geochronometer and can potentially be used to constrain the temperature of carbonatite formation (e.g., Andersen and Austerheim, 1991; Tappe et al., 2009; Liu et al., 2018).

Numerous publications describe the paragenetic relations and major-element composition of micas at specific localities (notably, Rimskaya-Korsakova and Sokolova, 1964; Gaspar and Wyllie, 1987; Heathcote and McCormick, 1989; Brigatti et al., 1996; McCormick and Le Bas, 1996; Seifert et al., 2000; Viladkar, 2000; Brod et al., 2001; Lloyd et al., 2002; Lee et al., 2003; Cordeiro et al., 2010; Krüger et al., 2013; Guarino and Brigatti, 2018). Surprisingly, however, no systematic study of trace-element variations or zoning in carbonatitic micas has been attempted to date. Although the importance of

careful analysis of zoning patterns has been underscored in many publications (Gaspar and Wyllie, 1982; McCormick and Le Bas, 1996; Viladkar, 2000; Brod et al., 2001; Lee et al., 2003; Ying et al., 2003), none of them discuss trace-element distributions or provide much comparative context. Overall, if we disregard bulk analyses of monomineralic concentrates, reliable trace-element data for carbonatitic micas are virtually limited to a few recent laser-ablation studies (Reguir et al., 2009; Milani et al., 2017). It is also noteworthy that the majority of pre-2005 publications lack data on F and Cl, and some report unusually high abundances of certain "uncharacteristic" elements (e.g., up to 0.27 *wt*.% NiO in Ying et al., 2003). In the absence of reported detection limits, it is not clear whether such data should be treated as reliable.

The present contribution is aimed at addressing these knowledge gaps and complementing the existing literature on non-carbonate minerals from carbonatites and their petrogenetic significance (Chakhmouradian and Zaitsev, 2002; Reguir et al., 2008, 2009, 2012; Chakhmouradian et al., 2017). Our primary objectives are: (1) to provide a paragenetic context for mica-group minerals in carbonatites and related rocks; (2) to advance the current understanding of the compositional variation of these micas (including trace-element distributions) using precise high-resolution analytical techniques; (3) to discuss the significance of compositional zoning and (4) its implications for elucidating the evolution of carbonatitic systems.

Research material and methodology

A suite of 57 carbonatite samples from 39 carbonatite complexes worldwide was selected for the present study. With a few exceptions (marked "loan" in Supplementary Table 1), this material was collected by the authors from bedrock outcrops and drill core ("core"). About 60% of the samples represent "classical" anorogenic intrusions emplaced in areas of intraplate or epicontinental rifting (Kramm et al., 1993; Rukhlov and Bell, 2010). Three of these (Shaxiongdong in China, Vishnevye Gory in Russia and Aley in Canada), located in plate-margin settings, were affected by collisional deformation and low-grade metamorphism long after their emplacement (Xu et al., 2008; Nedosekova et al., 2013; Chakhmouradian et al., 2015). Nine localities represent carbonatites from plate-collision zones; their origin is certainly linked to orogenic processes and, possibly, subduction (Castor, 2008; Chakhmouradian et al., 2008; Hou et al., 2015). These rocks are not as well-understood (in particular, with regard to their place in lithospheric evolution) as their anorogenic counterparts. Four intrusions (Argor, Cargill, Goldray and Valentine Twp.) were emplaced in the long-lived (Neoarchean-Paleoproterozoic) Kapuskasing Uplift in the Slave craton, Ontario, Canada. Because this structure is variably interpreted as a crust-scale intracratonic thrust, transcurrent shear zone and Paleoproterozoic rift (see discussion in Bursnall et al., 1994), and carbonatitic magmatism was recurrent throughout the Uplift from ~1.9 to ~1.1 Ga (Rukhlov and Bell, 2010), the tectonic setting of these four complexes is recorded as "debatable" (Supplementary Table 1). Finally, one sample of intrusive calcite carbonatite from Fuerteventura Island in the Canaries (de Ignacio et al., 2006) was also investigated.

Polished thin sections were prepared and examined using polarizing microscopy, back-scattered-electron (BSE) imaging and energy-dispersive X-ray spectrometry to determine their microtextural characteristics, paragenetic interrelations of micas with other minerals, and to prepare detailed sample

maps for further analysis. The abundances of major and minor elements (~850 points) were quantified using wavelength-dispersive X-ray spectrometry (WDS) with a Cameca SX100 automated electron microprobe. The instrument was operated at an accelerating voltage of 15 kV and a current of 20 nA, with a beam defocused to 10 μm. Other instrumental parameters, including standards employed for calibration, analytical lines, WDS detector types and lower detection limits, are listed in Supplementary Table 2.

The abundances of selected trace elements (~820 analyses) were measured by laser-ablation inductively-coupled-plasma mass-spectrometry (LA-ICPMS) using a 213-nm Nd-YAG Merchantek laser connected to a Thermo Finnigan Element 2 sector-field mass-spectrometer at the University of Manitoba. The data were collected using spot analysis with a 30-40 μm beam and the laser-energy density between 2.5 and 5.17 J/cm^2. Matching BSE and reflected-light images of the areas analyzed by WDS were used to accurately position a laser beam on the sample. Ablation was done in Ar and He atmospheres. Oxide production rate was monitored during instrument tuning by measuring ThO/Th ratio and maintained below 0.2%. Synthetic glass standard NIST 610 (Norman et al., 1996) was employed for calibration and quality control. All analyses were performed in a low-resolution mode (~300) using Pt skimmer and sample cones. Data reduction was carried out online using the IOLITE software, version 3.63 (Woodhead et al., 2007). The Si concentrations determined by WDS were used as an internal standard for all analyses. The quality control was achieved by carefully selecting the portion of the laser signal that kept fractionation at less than 10% and fractionation/error ratio at less than three. A complete list of measured isotopes and their typical lower limits of detection is provided in Supplementary Table 2.

Micas in carbonatites and related rocks: an overview

Dark-colored trioctahedral micas

By far the most common silicate constituent of calcite and dolomite carbonatites is dark-colored trioctahedral micas (DTM), which correspond to a complex solid solution between phlogopite [$K(Mg,Fe)_3(AlSi_3O_{10})(OH)_2$], annite [$K(Fe,Mg)_3(AlSi_3O_{10})(OH)_2$], fluorophlogopite [$K(Mg,Fe)_3(AlSi_3O_{10})F_2$], tetra-ferriphlogopite [$K(Mg,Fe)_3(FeSi_3O_{10})(OH)_2$] or, in some cases, kinoshitalite [$Ba(Mg,Fe)_3(Al_2Si_2O_{10})(OH)_2$] (see below). McCormick and Heathcote (1987) described reaction rims on phlogopite xenocrysts from Perryville and Brazil Branch carbonatites in Arkansas (USA), which they identified as eastonite [ideally, $K(Mg_2Al)(Al_2Si_2O_{10})(OH)_2$]. However, these authors also commented on (but did not quantify) high Ba levels in their samples, and on the uncertainty of Ti measurements in the presence of Ba. Our recalculations of the McCormick and Heathcote's (1987) data show that the Arkansas material has a large (up to 20%) deficiency in the K site, which correlates positively with the Al content, and that the proportion of octahedrally coordinated Al does not exceed 0.22 atoms per formula unit (apfu). Thus, we suggest that this mica is not eastonite, but probably a member of the phlogopite-kinoshitalite series.

In plutonic rocks, the relative abundance and morphology of DTM vary greatly along with textural variations. Euhedral platy, stubby prismatic or, less commonly, columnar crystals occur in isolation, or form stacked clusters in a carbonate mesostasis, often in association with apatite and magnetite. Their

size is typically commensurate with the character of the host rock, and crystals measuring several cm across are not unusual in coarse-grained calcite carbonatites (Fig. 1a). Where clinopyroxenes or amphiboles are present, phlogopite appears to crystallize after, and locally replace, these minerals (e.g., Figs. 1h, 2d in Reguir et al., 2012). Paragenetic relations with magnetite are less clear, although in the majority of cases, this mineral appears to predate, or be nearly contemporaneous with, DTM. Crystallization spans of apatite and DTM overlap, judging from the presence in the latter of apatite inclusions (Fig. 1b) that are sometimes confined to the margin of mica crystals (Fig. 1c). Phlogopite and related species typically increase in abundance (locally gaining the status of a rock-forming constituent) in:

(1) The selvages of carbonatite bodies, at their contact with metasomatized silicate wall-rocks (Fig. 1d-g), particularly if the latter are rich in ferromagnesian silicates or K-feldspar. Here, DTM form interlocking subhedral crystals fringing the contact and projecting inwards; typical associated minerals are apatite and alkali-rich amphiboles. Large carbonatite bodies may be enveloped in essentially monomineralic micaceous rocks that are referred to as glimmerite (Heinrich, 1970; Morbidelli et al., 1986; our Figs. 1g, 2a) or, in some publications, as phlogopitite (Brod et al., 2001; Cordeiro et al., 2010). Note that the former name implies an igneous origin, whereas "phlogopitite" is, strictly speaking, a metamorphic term (Fettes and Desmons, 2007, p. 14; Raith et al., 2008). Neologisms, like phlogopitelite (Han et al., 2018), are unwarranted and should not be proliferated in the literature. In exocontact fenites, DTM may still be an abundant component, but are associated with increasing proportions of other metasomatic phases (in particular, albite, potassium feldspar, muscovite, alkali-rich amphiboles and clinopyroxenes) and relict minerals inherited from the precursor rock. Relations between carbonatites, glimmerites and fenites are discussed in Elliott et al. (2018).

(2) Reaction rims surrounding xenoliths and xenocrysts derived from silicate wall-rocks (Fig. 2b, c). A glimmerite zone is developed concentrically around the wall-rock fragment, often in association with Na-rich amphiboles. The thickness of glimmeritic rind may vary significantly among similar xenoliths within the same outcrop (Fig. 2c) because it depends on the distance of their transport, their cohesiveness, etc.

(3) Silicate-oxide-apatite-rich rocks spatially associated with carbonatites. In the majority of cases, these rocks are viewed as genetically related to each other owing to their shared mineralogical, structural and trace-element characteristics. The most common variety are cumulate units enriched in magnetite, apatite, mafic silicates, niobates and baddeleyite or zircon (Fig. 2d). For the purposes of this study, we include phoscorites in this category (Fig. 2e), although both crystal fractionation and liquid immiscibility have been invoked to explain the genesis of these rocks (Krasnova et al., 2004). Because we did not observe any evidence of immiscibility in our samples, we contend that gravitational settling of forsterite, magnetite, apatite and baddeleyite (all denser than 3 g/cm^3) is the most intuitive explanation for this mineral association. The modal content of DTM in phoscorites varies widely (Krasnova et al., 2004; Lee et al., 2004; Cordeiro et al., 2010), reaching 60 vol.% in some complexes (e.g., Milani et al., 2017), although it

is debatable whether something with this much mica and little forsterite or magnetite should be referred to as phoscorite vis-à-vis the original definition of Russell et al. (1955).

(4) Layers and stringers in deformed carbonatites. Differences in the mechanical properties of silicate and carbonate minerals and the susceptibility of the latter to ductile flow produce inequigranular, modally heterogeneous foliated rocks (Chakhmouradian et al., 2016; Cerva-Alves et al., 2017). Crystals of DTM are crudely aligned with the foliation defined largely by grain-size variations, and concentrated in fine-grained, silicate-apatite-rich domains (Fig. 2f). With increasing strain, micas become bent or corrugated, develop strong drape-like extinction and morph into lozenge-shaped porphyroclast fish similar to those in mylonites (ten Grotenhuis et al., 2003; our Fig. 2g).

In extrusive and subvolcanic rocks, DTM may occur as (micro)phenocrysts, groundmass grains, or both (Ying et al., 2004; Tappe et al., 2006, 2009; Chakhmouradian et al., 2009; de Ignacio et al., 2012; Krüger et al. 2013; Campeny et al., 2015; Savelyeva et al., 2016). Note that it is not always possible to determine unambiguously whether large mica crystals in pyroclastic and diatreme facies represent phenocrysts or xenocrysts (Eby et al., 2009). Both massive and phlogopite-phyric rocks may be present within the same area (Savelyeva et al., 2016). The form of mica occurrence does not seem to correlate with the bulk composition of its host rock (Fig. 3), i.e. some low-(K, Mg, Al, Si) carbonatites have been reported to contain phenocrystic DTM (Campeny et al., 2015). Phenocrysts commonly show evidence of plastic deformation and two or more growth episodes separated by resorption (Fig. 4a, b).

Phlogopite and related minerals are generally unstable in hydrothermally overprinted carbonatites, which include rocks modified by deuteric fluids, basinal brines and metamorphism. Typical alteration products are clinochlore, serpentine and dolomite, whereas serpentine, muscovite, microcline (usually associated with dolomite), talc, calcite and quartz are less common (Fig. 4b-e). It is noteworthy that incipient replacement of DTM by chlorite and other secondary phyllosilicates may not be readily detectable using techniques with a spatial resolution of >1 μm. The precursor mineral and its alteration product(s) may be interstratified on a nanoscale (Veblen and Ferry, 1983; Olives Baños and Amouric, 1984), resulting in lower average atomic number (AZ) in BSE images, K deficiency and low analytical totals in electron-microprobe analyses (e.g., Andersen, 2008). Without transmission-electron microscopy studies, it is impossible to say whether these low-K compositions represent cation-leached and hydrated micas transitional to vermiculite [$(Mg,Fe,Al)_3(Al,Si)_4O_{10}(OH)_2 \cdot nH_2O$], or mixtures of different phyllosilicates (cf. Figs. 4d and 4f). Commercially viable deposits of vermiculite associated with carbonatite-phoscorite complexes occur at Palabora in South Africa, Kovdor, Seblyavr and Vuorijarvi in Russia, and Qieganbulake in China (Heinrich, 1970; Afanasyev, 2011; Han et al., 2018). There is no doubt that these deposits developed at the expense of glimmerites or other DTM-rich rocks, but the mechanisms and conditions of vermiculitization (i.e., hydrothermal vs. supergene) remain poorly understood.

Other micas

Tainiolite [$K(Mg_2Li)Si_4O_{10}F_2$] is an exceedingly rare light-colored mica that was reported from intrusive calcite carbonatites at Dicker Willem (Namibia) and Chuktukon (Russia), dolomite carbonatites from

Araxá (Brazil) and Akitskiy (Russia), and from silicic country rocks metasomatized near the contact with carbonatite intrusions at Magnet Cove (USA), Haast River (New Zealand) and Dicker Willem (Miser and Stevens, 1938; Cooper et al., 1995; Traversa et al., 2001; Sotnikova and Vladykin, 2008; Sharygin, 2017). This mineral has also been tentatively identified in dolomite-calcite carbonatitic lava from São Vicente (Cape Verde), although its Li content has not been quantified (de Ignacio et al., 2012). Tainiolite can be distinguished from DTM by its lack of pleochroism, higher SiO_2, MgO and F contents (>56, 18 and 6 wt.%, respectively) at generally low levels of Al and Fe (Supplementary Table 3).

Muscovite is a common mineral in carbonatite complexes, although its petrogenetic significance has not been fully appreciated, and data available on its composition and paragenetic relations are scarce. Felsic rocks in exocontact zones and xenoliths entrained in carbonatites commonly contain fine-grained aggregates of muscovite, calcite and albite, hyalophane or celsian (± DTM, chlorite and epidote-group minerals) developed after primary feldspars and feldspathoids (Figs. 1e, 4g, 4h). This type of replacement process, often referred to as sericitization, may affect a wide range of country rocks (from mafic to felsic) or alkaline silicate (typically, syenitic) units coeval with the carbonatite (Currie and Ferguson, 1971; Cooper, 1996; Gwalani et al., 2010; Cooper et al., 2011, 2016). Replacement of plagioclases by muscovite (± DTM, hyalophane) implies significant loss of K from carbonatitic magma into its silicate wall-rock. It is noteworthy that there is no consensus on the role of muscovite in fenitization processes. Le Bas (2008) observed that the onset of fenitization at Silai Patti (Pakistan) is marked by the disappearance of muscovite from country rocks, whereas Gwalani et al. (2010) reported that the *appearance* of this mineral is indicative of contact metasomatism at Yungul (Australia). Quantitative data available for muscovite from these parageneses are very limited. Some of the samples examined in the present work (Supplementary Table 3) contain relatively high Mg and Fe contents (up to 2.6 wt.% MgO and 6.7 wt.% Fe_2O_3), but low levels of Ba. Up to 2.3 wt.% BaO was reported in muscovite associated with Ba minerals in fenites from the Haast River area (Cooper, 1996; Cooper et al., 2016). Another dioctahedral mica, celadonite [$K(Mg,Fe,Al)_2Si_4O_{10}(OH)_2$] was reported as a secondary mineral developed after ferromagnesian silicates in the Araxá carbonatites, Brazil (Traversa et al., 2001).

Compositional variation of DTM

Major elements

In carbonatites and associated cumulate rocks, DTM cover a wide range of compositions (Supplementary Tables 4-7). Those closest to the end-member phlogopite (i.e. 2.7-2.9 apfu Mg and ~1 apfu $^{[4]}Al$) occur in phoscorites (Kovdor, Aley) and early calcite carbonatites, typically in association with forsterite and magnetite (Kovdor, Jacupiranga in Brazil, Fengzhen in China: Fig. 5a). Micas with the highest Fe/(Fe+Mg) ratio (up to 0.6), corresponding to annite, rim phlogopite at Prairie Lake (Canada) and Shaxiongdong; however, unzoned euhedral crystals of annite (1.4-1.7 apfu Fe and 0.9-1.4 apfu Mg) were also observed in calcite carbonatites from Bayankol (Tuva, Russia), Spanish River and Cinder Lake (Canada). The Al content of studied micas is highly variable (Fig. 5a, b), commonly within the same crystal due to zoning (see below). As can be expected, the lowest Al values (ca. 0.1-0.2 apfu) are observed in the tetra-ferriphlogopite rim of strongly zoned crystals from Kovdor and Guli (Russia), where the content of this element is insufficient, and Fe^{3+} is required, to compensate Si deficiency in the

tetrahedrally coordinated sites (Supplementary Table 4). The $^{[IV]}Fe^{3+}$-for-$^{[IV]}Al$ substitution is discussed in more detail below, in Section 4.5. The highest levels of Al (1.8-2.0 apfu), most of which (85-87%) is tetrahedrally coordinated, occur in the Ba-rich rims of phlogopite from Iron Hill (USA), where the "surplus" of Al compensates K^+ substitution by Ba^{2+} (Supplementary Table 5). The proportion of octahedrally coordinated $^{[VI]}Al$, indicating a solid solution towards eastonite, does not exceed 0.3 apfu (estimated based on stoichiometry) and reaches this maximum level in the Iron Hill and Cinder Lake samples (15% and 20% of the total Al, respectively).

Manganese, Ti and Ba occur in DTM in variable concentrations, ranging from trace levels to >>1 wt.%. Because a large proportion of the studied samples contain <1,000 ppm of these elements (~55% of the Mn LA-ICPMS data and ~40% of the Ti and Ba measurements), their distribution and variations will be discussed in Sections 4.2 and 4.3 below.

The lowest levels of F are observed in samples from Kovdor phoscorites (≤0.07 apfu), whereas the majority of DTM (including those from Aley phoscorites, Kovdor and Jacupiranga carbonatites) contain 0.1-0.4 apfu F (i.e., ≤1.8 wt.%; Fig. 5c). Micas from calcite carbonatites at Fengzhen, Mountain Pass (USA), Aley, Carb Lake and Eden Lake (Canada), as well as Aley cumulates, contain 0.8-1.0 apfu F and thus approach the phlogopite – fluorophlogopite boundary. Somewhat lower levels (0.6-0.8 apfu F) are found in phlogopite from norsethite-dolomite carbonatite at Bayan Obo (China). Fluorophlogopite sensu stricto (up to 8.5 wt.% or 1.9 apfu F) occurs in calcite carbonatites from Maoniuping, Muluozhai and Lizhuang (Sichuan, China) and Kamthai (India). It is noteworthy that all of the latter four, Bayan Obo and Mountain Pass host (sub)economic REE mineralization. Fluorine-rich micas in the Sichuan, Kamthai, Carb Lake and Eden Lake rocks are associated with fluorite, whereas this mineral was not observed in any significant quantity in the Fengzhen, Mountain Pass or Aley samples. Note also that in addition to localities, where DTM are represented exclusively by phlogopite or fluorophlogopite (e.g., Kovdor and Maoniuping, respectively), there are cases where both may be present depending on their paragenesis. For example, at Saint-Honoré (Canada), dolomite carbonatites contain phlogopite (0.2-0.3 apfu F), whereas micas from fluorite-rich rocks hosting Nb mineralization are high in F (0.9-1.3 apfu).

Chlorine levels are very low in all studied samples, typically not exceeding its detection threshold by WDS (Supplementary Table 2). The maximum Cl content (0.3 wt.% or 0.04 apfu) was recorded in phlogopite from the Saint-Honoré dolomite carbonatites, which are unusual in containing abundant halite (Kamenetsky et al., 2015).

Minor and trace elements: large interlayer cations

Sodium is a ubiquitous substituent in DTM, but its concentrations usually do not exceed 0.1 apfu (i.e., ~0.7-0.8 wt.% Na_2O). Higher levels (0.1-0.2 apfu), producing the leftward spread among low-Ba compositions in the K vs. Ba diagram (Fig. 5d), were detected in some samples from early phoscorites and carbonatites at Aley, Kovdor and Sokli (Finland). These Na-enriched samples lack clinopyroxenes and amphiboles, which have a greater structural capacity for Na than DTM, although there are also many examples of early clinopyroxene- and amphibole-free carbonatites that contain low-Na phlogopite (e.g., ≤0.05 apfu at Oka and Jacupiranga). Moreover, within the same complex, phlogopite from temporally

distinct, but mineralogically similar units may exhibit wide variations in Na (e.g., 0.08-0.26 and 0.06-0.08 apfu in carbonatites KV-7 and KV-226, respectively).

Within the examined sample set, Ba concentrations vary over five orders of magnitude, from below detection by LA-ICPMS to 12.7 wt.% BaO, which is equivalent to 38 mol.% kinoshitalite (Fig. 5d); Supplementary Table 5). Intragranular variation in Ba content may reach two-three orders of magnitude in some micas (see Section 4.5). The highest levels of this element are observed in samples from calcite-dolomite carbonatite at Iron Hill, whereas the lowest abundances (<10 ppm) in the rim of phlogopite associated with barite at Mountain Pass. Strontium is a trace substituent in most of the studied DTM (Table 1), although several samples of calcite carbonatite (Aley, Wekusko Lake, Argor and Goldray in Canada; Jacupiranga, Guli, Shaxiongdong and Maoniuping) show Sr levels below or at the level of its detection by LA-ICPMS (≤3 ppm). The highest concentrations of this element (450-830 ppm) are found in Ba-rich phlogopite from Iron Hill. Most of the analyzed micas exhibit a positive correlation between their Ba and Sr contents that either increase or decrease from the core rim-wards (Fig. 6a), although there are a few exceptions (see Section 4.5). For example, relatively Ba-rich compositions from Aley and Oka (2.1-2.7 and 1.2-1.9 wt.% BaO, respectively) contain elevated Sr levels (~150-200 ppm) comparable to those in Ba-poor phlogopite from Prairie Lake (0.4-0.6 wt.% BaO). Notably, all carbonatites from orogenic settings contain DTM with very low Sr levels (<25 ppm).

Rubidium and Cs are present at trace levels in all of the studied samples. Their concentrations vary over two orders of magnitude (10 to 1250 and <0.6 to 52 ppm, respectively), and do not appear to correlate with the tectonic setting of host rocks (Table 1). The majority of micas (~75% of the LA-ICPMS data) contain 150-650 ppm Rb and 3-20 ppm Cs. Although many samples show positive correlation between these two elements (e.g., Mountain Pass, Fuerteventura, Guli, Shaxiongdong), there are also cases where one of them decreases or increases in abundance from the core of mica crystals rim-ward whereas the other does not (Fig. 6b; see also Section 4.5). The highest levels of Cs (38-52 ppm) are found in the rim of phlogopite crystals fringing the fenitized contact between syenite and calcite carbonatite at Eden Lake (Fig. 1d).

The concentrations of Y, lanthanides, Th and U are invariably low (≤4, 7, 6 and 3 ppm, respectively), even in micas from carbonatites strongly enriched in these elements (e.g., Mountain Pass, Bayan Obo and Maoniuping). Note also that 95% of the data show <4 ppm rare-earth elements (REE = Y + La…Lu), 0.25 ppm Th and 0.5 ppm U. Also, higher abundances of these elements tend to be found in isolated analyses, rather than being consistently observed in specific samples or zones; e.g., only two out of 21 LA-ICPMS measurements of the Prairie Lake micas gave 6-7 ppm REE, whereas the rest show <2.5 ppm. These observations strongly suggest that the sporadically observed “enrichment” of DTM in REE, Th or U arises from ablation of unidentified micro-inclusions of accessory phases. Typically, the Pb abundances are also low (≤1.7 ppm in 85% of the data), but three notable exceptions, which *consistently* show elevated levels of this element, are samples from Mountain Pass, Maoniuping and Fengzhen (12-374, 6-27 and 9-14 ppm, respectively). Interestingly, all three represent orogenic tectonic settings. The large variations in Pb in the Mountain Pass phlogopite are addressed below.

Minor and trace octahedral cations: transition metals

Titanium and Mn are ubiquitous substituents in DTM; their concentrations vary by about two orders of magnitude, reaching maximum values in calcite carbonatites at Bayankol (5.7 wt.% TiO_2) and Fuerteventura (2.0 wt.% MnO), respectively. However, low-Ti and -Mn compositions are far more common, with ~60% of the Ti and >90% of the Mn data falling below 5,000 ppm. There is no clear correlation between either Ti or Mn levels and tectonic setting. Variations in both elements exceed one order of magnitude in some zoned micas (see Section 4.5).

Scandium abundances are typically low (85% of the measured values are <15 ppm), but occasionally reach much higher levels: i.e., up to 30 ppm at Aley, 50 ppm at Jacupiranga, 60 ppm at Iron Hill and 280 ppm at Kovdor. Notably, all DTM with elevated Sc occur in anorogenic carbonatites; those from orogenic settings contain ≤7 ppm Sc (Table 1). Vanadium is present in detectable concentrations in all studied samples, with values ranging over three orders of magnitude across the dataset. With one exception, elevated V levels (>150 ppm) are observed in micas from carbonatites lacking magnetite or containing a late-crystallizing generation of this mineral postdating mica. For example, V abundances range from 215 to 230 ppm in the core of phlogopite phenocrysts from Zibo (China), but decrease by a factor of 1.5 in the rim, precipitated contemporaneously with groundmass magnetite (Fig. 4a). Phlogopite from Alnö (Sweden), which contains 420-510 ppm V, is an exception because it is associated with abundant magnetite. It is noteworthy, however, that all ferromagnesian minerals in this calcite carbonatite contain unusually high levels of V (i.e., 350-540 ppm in clinopyroxene, 560-660 ppm in hastingsite and 3100-3400 ppm in magnetite: Reguir et al., 2012), implying overall enrichment of their parental magma in this element. Zoned micas commonly show concomitant depletion in Ti and V (Fig. 6c; Section 4.5).

Chromium and Ni range in concentration from nil to ~900 and 600 ppm, respectively, but some 90% of the data fall below 50 ppm Cr and 160 ppm Ni. As can be expected, enrichment in both these elements is observed in DTM from carbonatites representing primary mantle-derived melts, or those containing abundant forsterite and magnetite and thus derived from relatively primitive magmas. The maximum levels of Cr and Ni are observed in phlogopite phenocrysts from the Zibo calciocarbonatitic diatreme of mantle origin (Ying et al., 2004). Compositionally heterogeneous micas commonly exhibit appreciable core-rim changes in Ni content, which may or may not correlate with Cr variations (Fig. 6d). Cobalt does not show consistent correlations with either Cr or Ni; the highest levels of this element are found in phlogopite from Goldray and Paint Lake, Canada (83-94 and 85-102 ppm, respectively). About 90% of the LA-ICPMS data have <50 ppm Co.

Minor and trace octahedral cations: high-field-strength elements

In the majority of samples, Zr is present at very low levels: 80% of all data fall below 20 ppm, and none of the samples from orogenic settings contain >14 ppm Zr. A few exceptions are the cores of zoned phlogopite crystals from Prairie Lake (33-52 ppm), Aley phoscorite (36-79 ppm), Zibo (160-170 ppm) and Valentine Twp. (160-200 ppm), and Ba-rich rims of micas from Oka and Iron Hill (20-61 and 31-105 ppm, respectively). Hafnium abundances in carbonatitic micas are typically <1 ppm, increasing to 1-2 ppm in the relatively Zr-rich samples from Prairie Lake, Aley and Valentine, and to 3.0-3.5 ppm at Zibo. Because of the low precision of Zr and Hf measurements at low concentrations, the Zr/Hf ratio could be reliably determined only for a small number of samples (Fig. 6e). The Zr/Hf values range from consistently

subchondritic in postorogenic carbonatites (<20 at Maoniuping, Lizhuang, Eden Lake and Paint Lake, and 13-29 at Fengzhen) to extremely superchondritic in a few other samples (97-123 at Valentine and 107-170 at Iron Hill).

Niobium is present in measurable concentrations in the majority of studied samples; the only exception is zoned crystals from Guli, where it was not detectable. As can be expected, the highest levels of this element are found in micas from carbonatites hosting niobate mineralization: ca. 200-350 ppm at Valentine and Vishnevye Gory, Russia; 200-580 ppm at Saint-Honoré; 430-940 ppm at Aley; 180-1070 ppm at Oka. However, micas from some carbonatites hosting pyrochlore are unremarkable in terms of their Nb content (e.g., 15-62 ppm at Sokli) and *vice versa*, i.e. some unmineralized rocks host Nb-rich mica (e.g., 260-560 ppm at Fuerteventura). Tantalum levels are generally low (~90% of the data fall below 25 ppm), but reach very high levels (50-160 ppm) in zoned crystals from the Aley phoscorite. None of the DTM samples from orogenic settings contain >70 ppm Nb or >3 ppm Ta. The Nb/Ta ratio could be determined in 85% of the samples (Fig. 6f) and shows extreme variations from consistently subchondritic (e.g., 5-8 at Zibo, 6-10 in the Aley phoscorite and 8-13 at Valentine) to strongly decoupled values (up to ~1400 at Vishnevye Gory and Bayan Obo, 1800 at Oka and Saint-Honoré, and 2000 at Shaxiongdong). Zoned micas commonly exhibit order-of-magnitude variations in Nb/Ta ratio (Fig. 6f).

Zoning in DTM from carbonatites

About 40% of the samples examined in the present work appear homogeneous in polarized light and BSE images or exhibit subtle compositional variations that do not conform to a particular pattern. Among the zoned DTM, the most common type by far (11 samples) is readily recognizable in thin section owing to the presence of a dark, reddish-brown (at maximum absorption) rim of variable thickness around a paler-colored core (Figs. 1b, 7a-c). The latter ranges in color (Y ≈ Z) from pale-green in relatively pure phlogopite (Fig. 7a) to greenish- or greyish-brown in Fe- and Ti-rich micas (Fig. 7b). Compositionally intermediate DTM are pleochroic from rose- or orange-brown (Y ≈ Z) to colorless (X). In some cases, the core-rim color contrast is so strong that it is also visible macroscopically (Fig. 1a). In most of the examined micas showing this zoning pattern, the reddish-brown material has an inverse absorption formula (X > Y ≈ Z; Fig. 7a) and is referred to hereafter as Type 1a zoning. In type 1a crystals, the core-rim boundary is irregular, and reddish-brown areas extend from the rim inwards along fractures and cleavage planes (Figs. 1b, 7a, 7c). In contrast, Type 1b crystals are characterized by normal absorption in their core and rim (Fig. 7b). Both normally and inversely pleochroic DTM are biaxial negative, length-slow with respect to their cleavage (i.e., X ≈ [001]) and have a small 2V angle (<15^{o}).

With a single exception (see below), the reddish-brown areas have a higher average atomic number (AZ) relative to the core in BSE images owing to their enrichment in Fe and Si, coupled with depletion in Mg and Al (Fig. 8a). Occasionally, core and rim may also show oscillatory variations in these elements that parallel the general trend (Fig. 7d). As can be seen from Figure 8a, the most extreme depletion in Al is observed in Type 1a micas from Kovdor and Guli, which evolve from phlogopite to tetra-ferriphlogopite (sensu stricto). The proportion of Fe^{2+} in these samples (calculated on the basis of stoichiometry) does not change much, whereas the Fe^{3+} content increases dramatically to compensate

the Si deficiency in the absence of sufficient $^{[IV]}Al$ (Fig. 8b). In the Kovdor and Guli samples, a transition from normal to inverse absorption occurs at ca. 0.3 apfu $^{[IV]}Fe^{3+}$.

Acknowledgements

This work was supported by the Natural Sciences and Engineering Research Council of Canada (NSERC), St. Petersburg State University (Pure ID 28160150, including Geomodel Research Center) and the Chinese National Science Foundation.

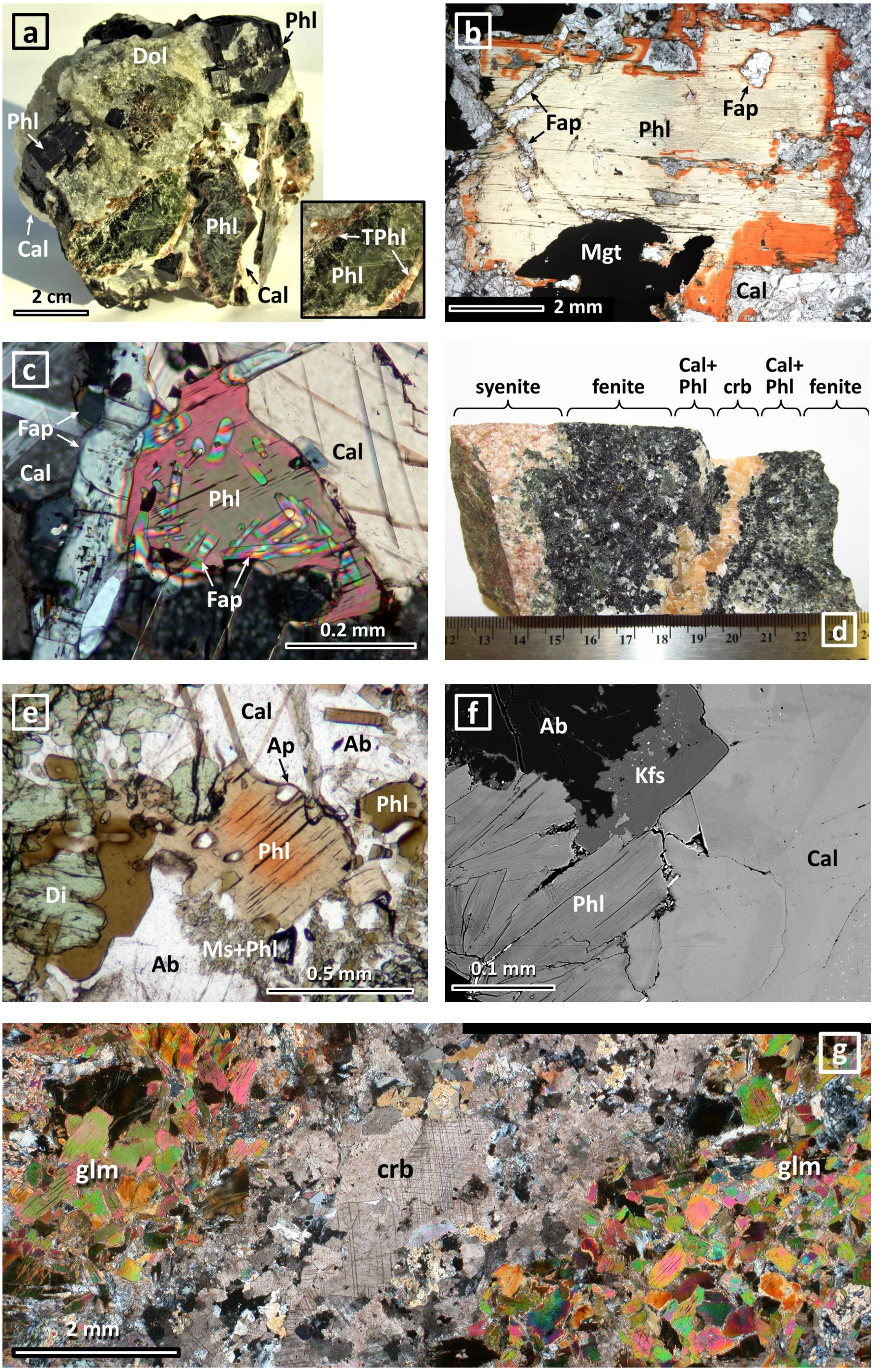

Fig. 1

Chakhmouradian et al., *Micas in carbonatites*

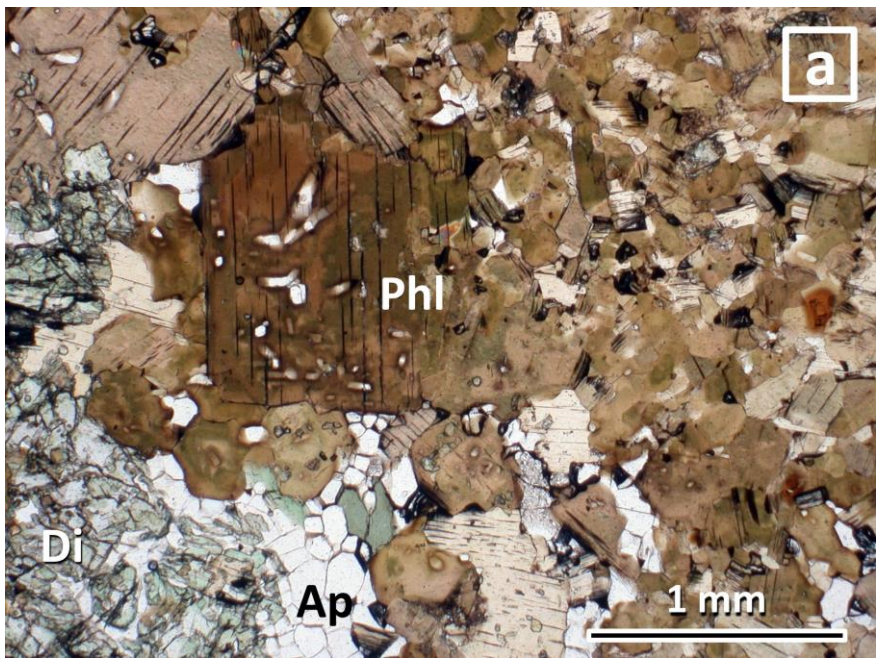

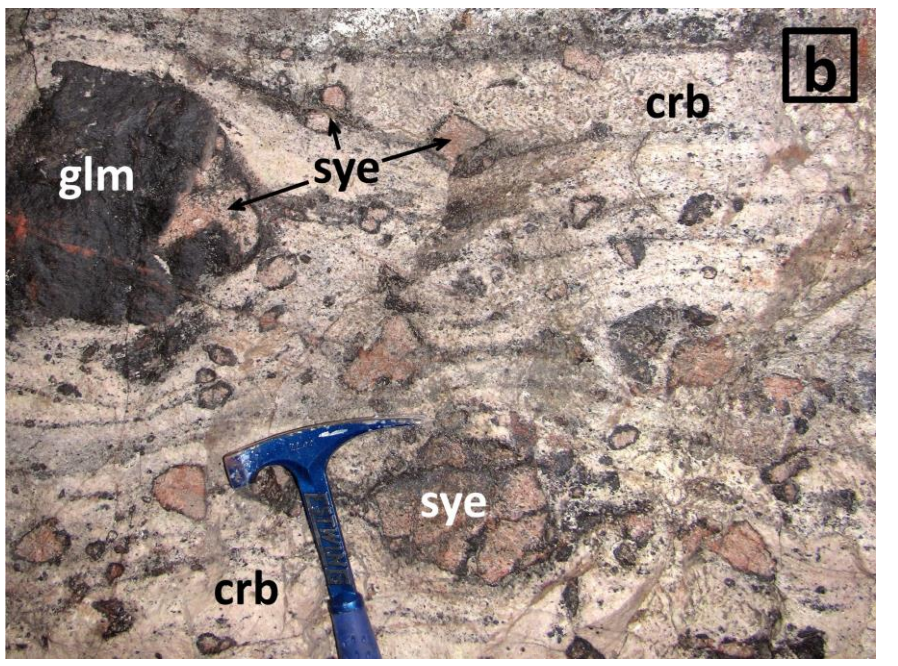

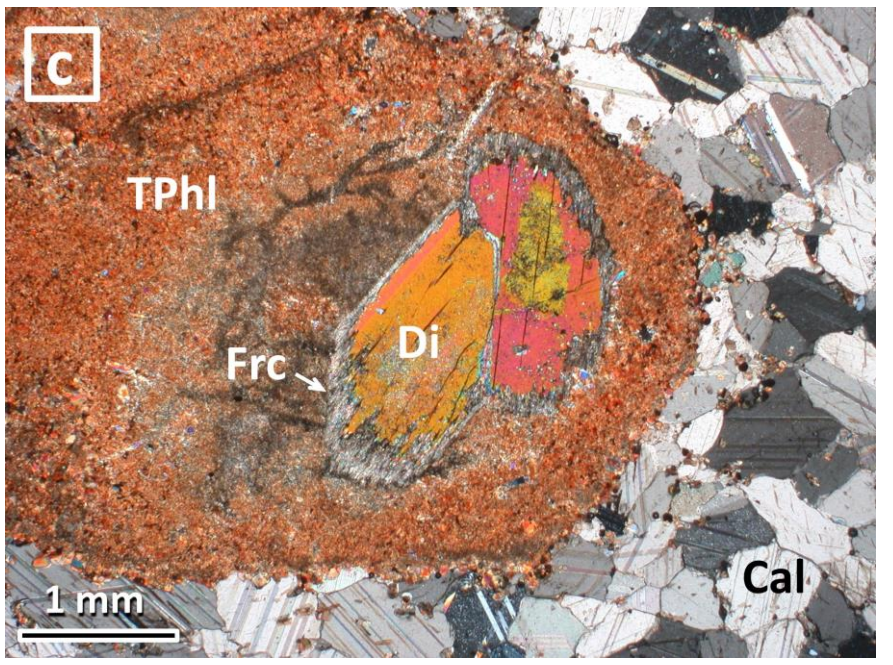

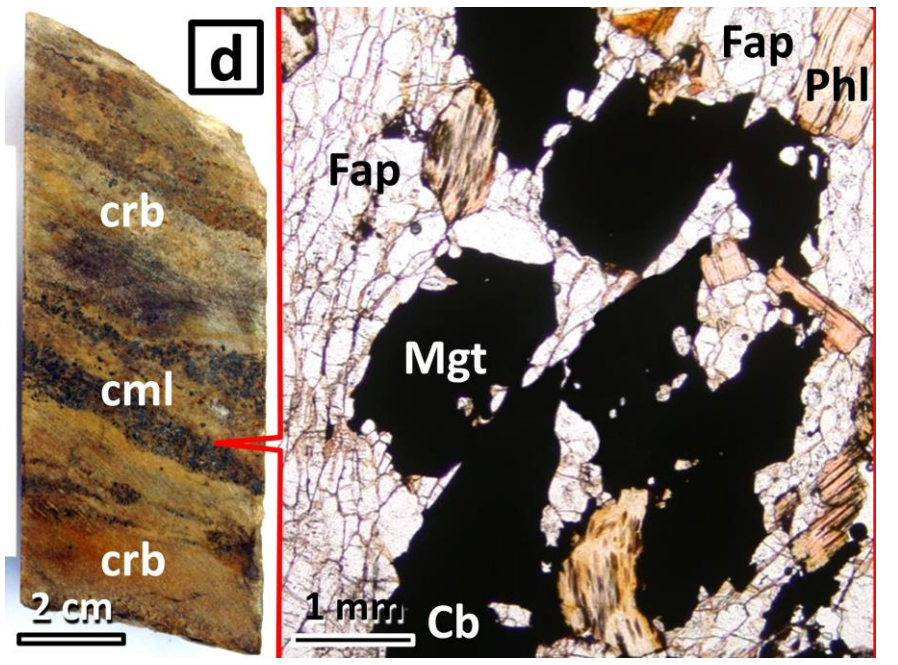

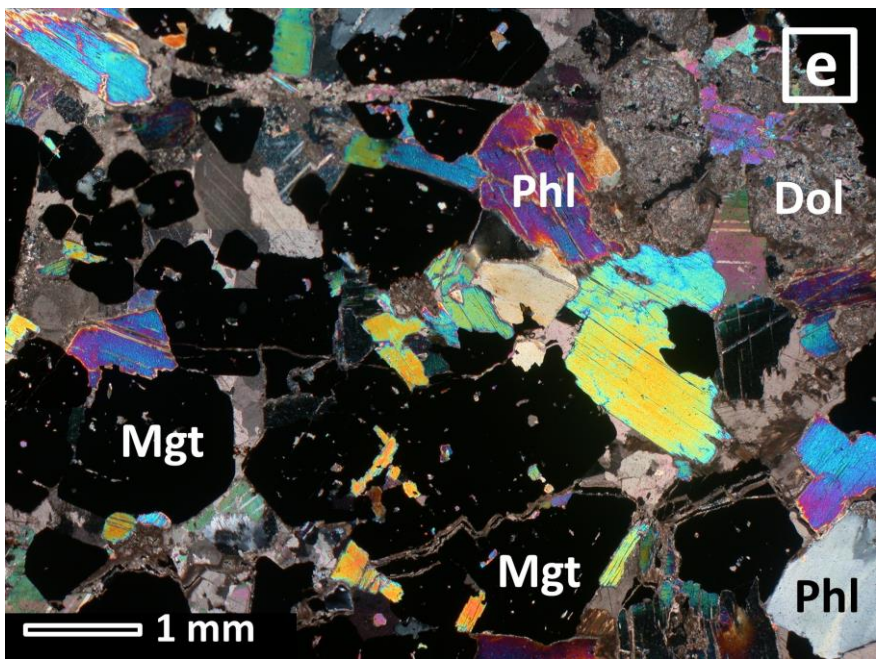

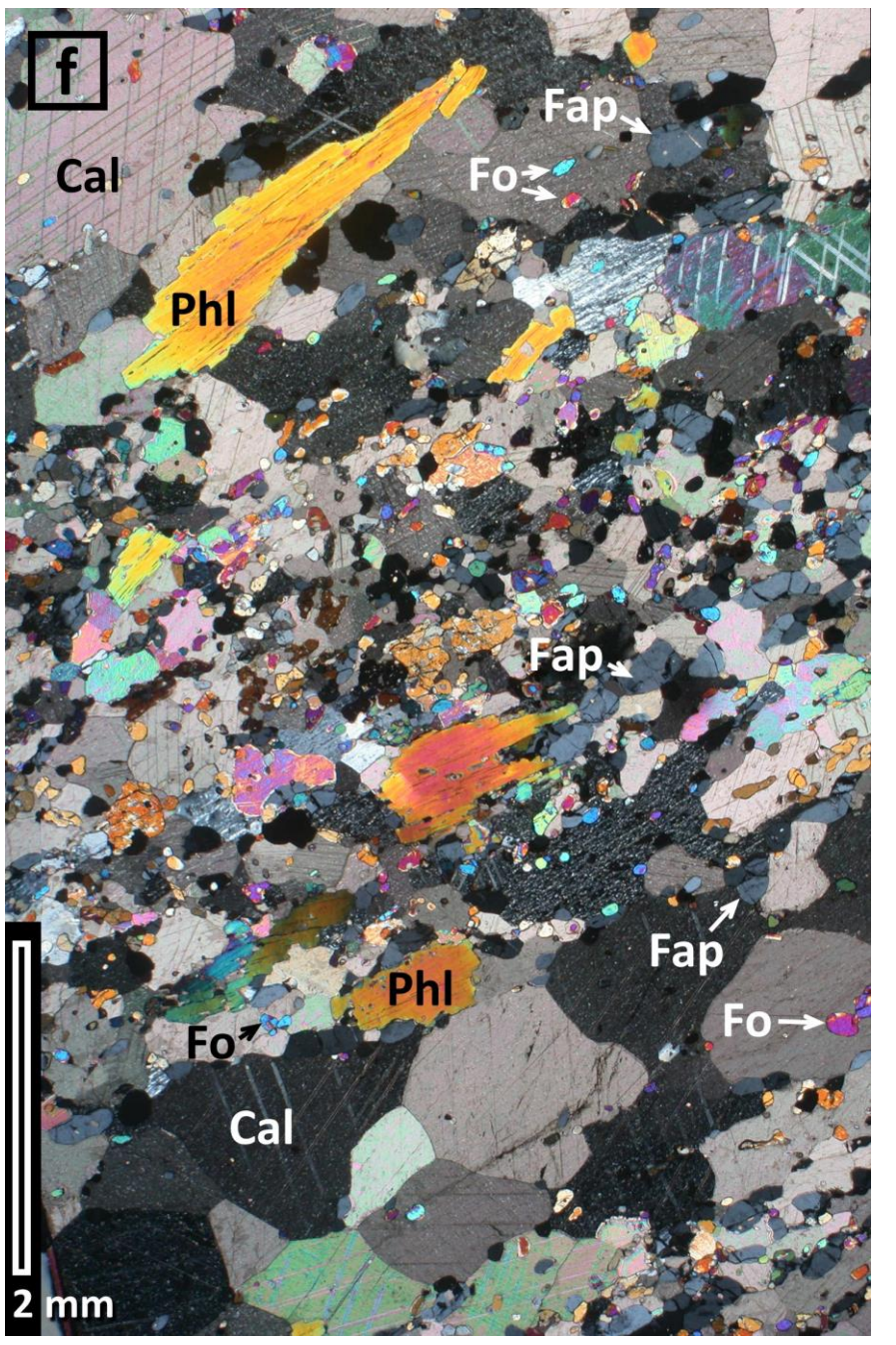

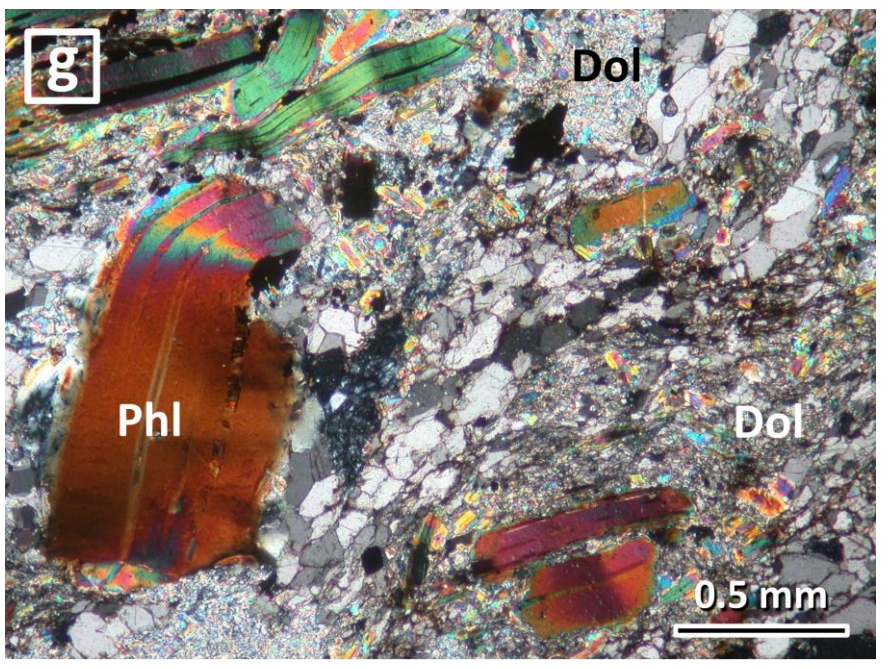

Fig. 2

Chakhmouradian et al., *Micas in carbonatites*

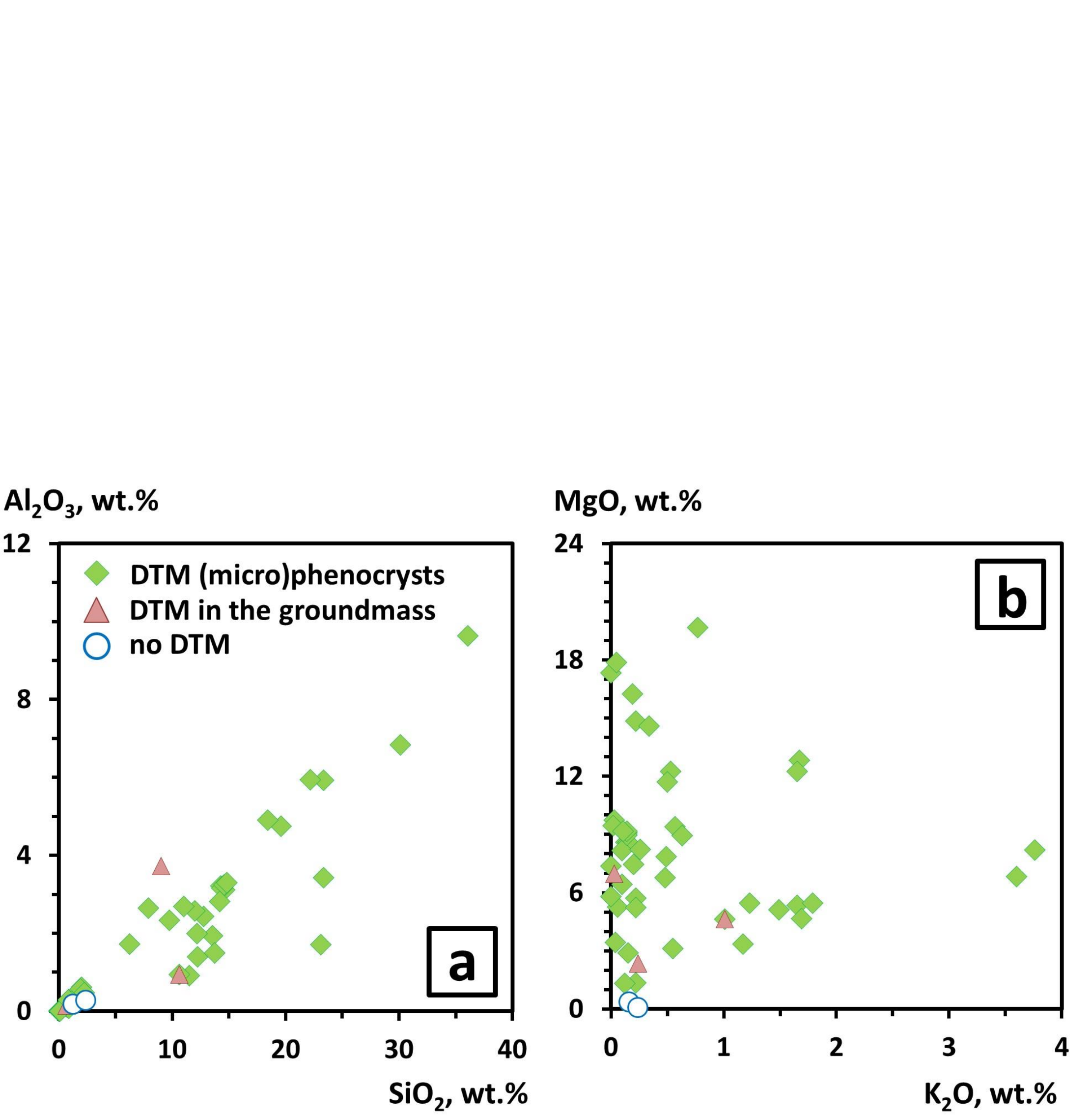

Fig. 3

Chakhmouradian et al., *Micas in carbonatites*

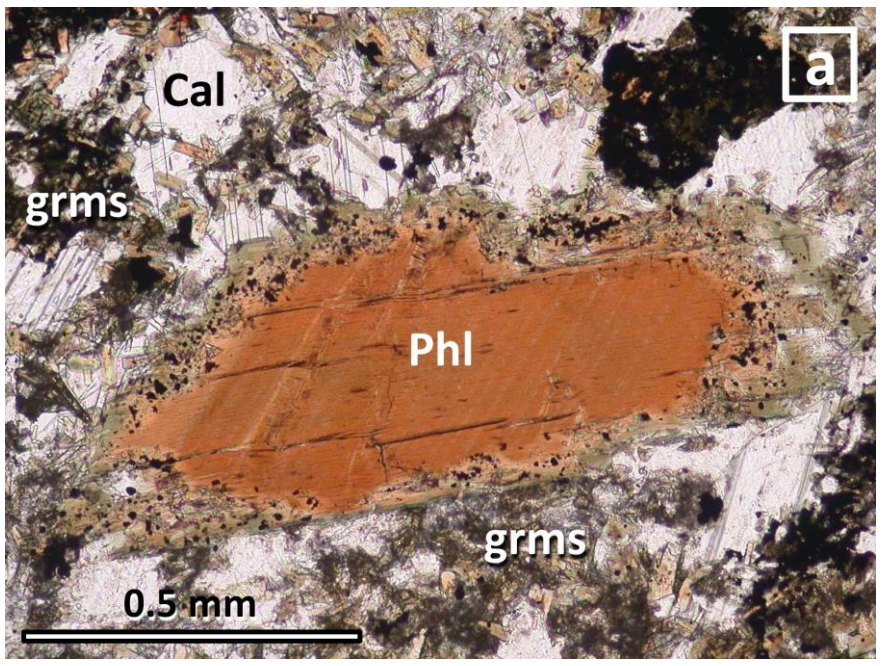

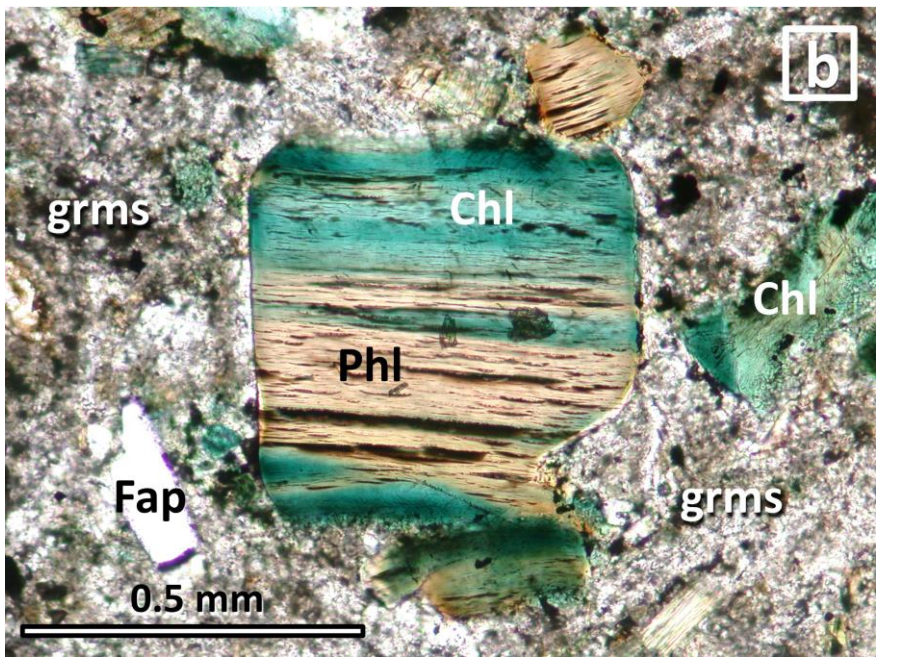

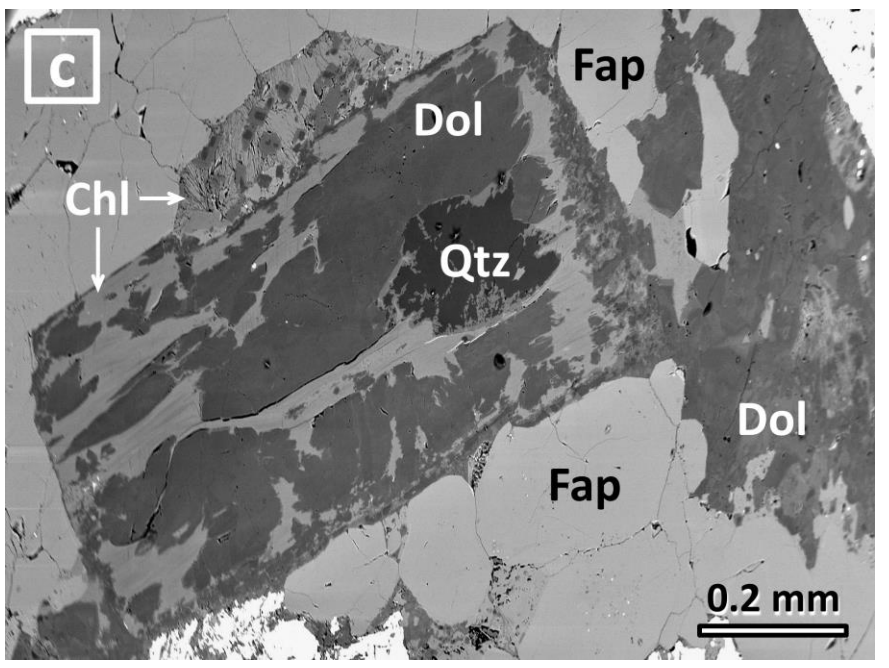

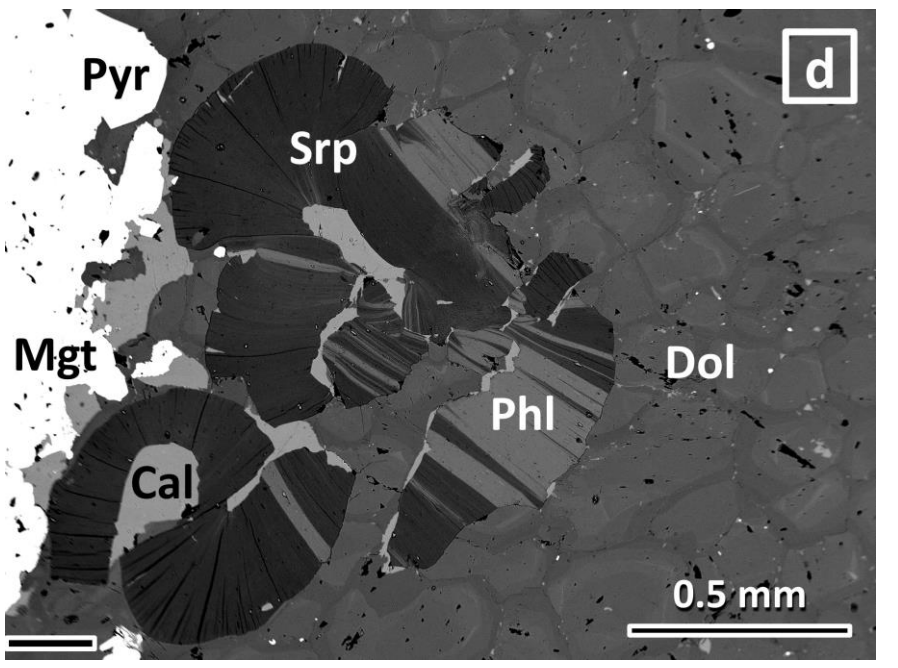

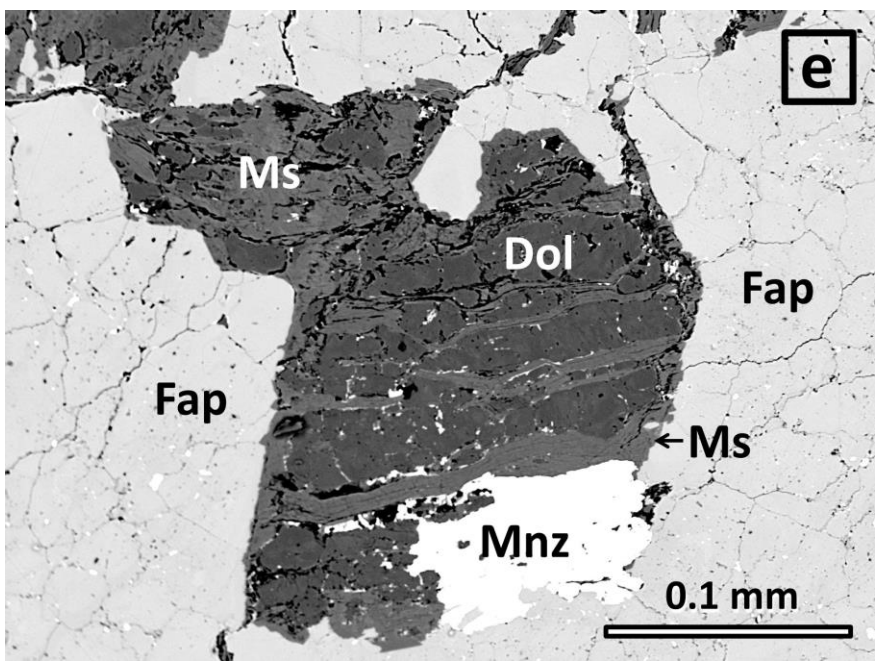

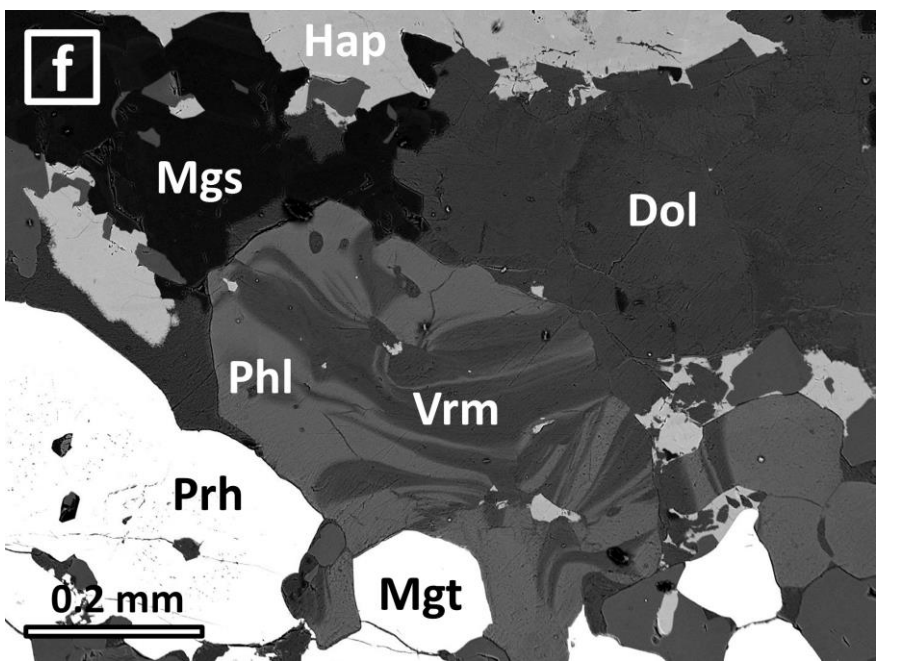

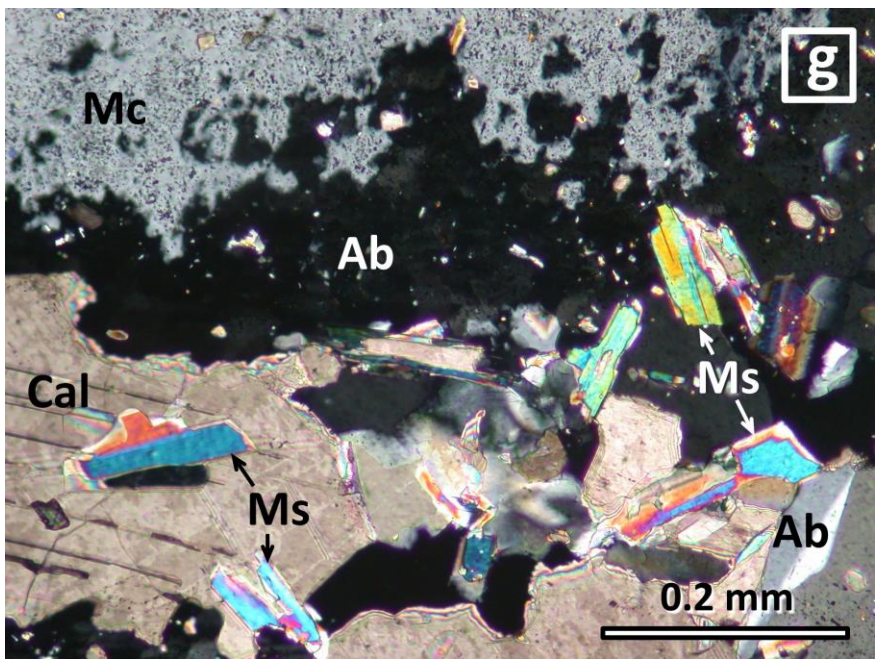

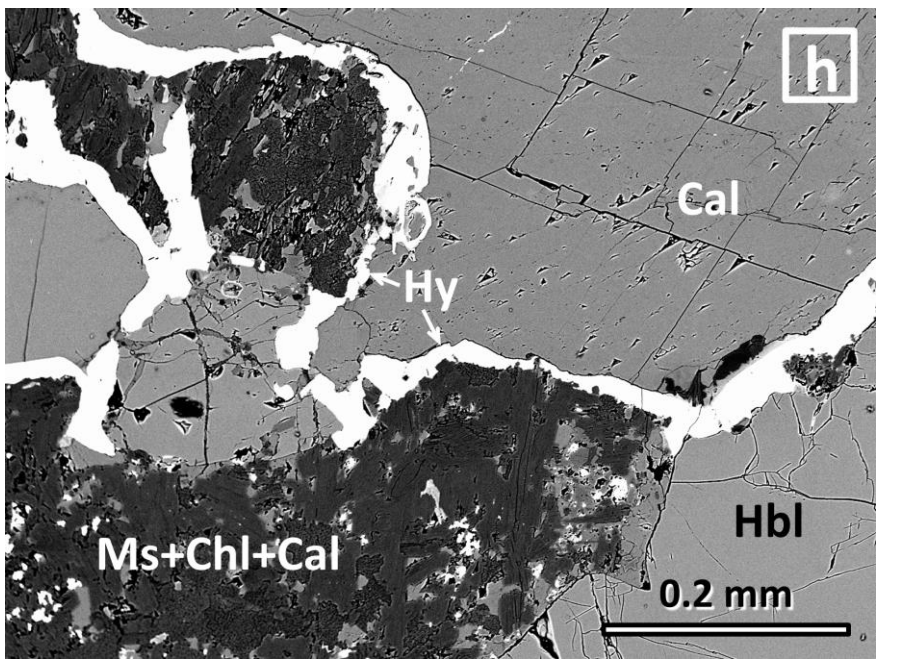

Fig. 4

Chakhmouradian et al., *Micas in carbonatites*

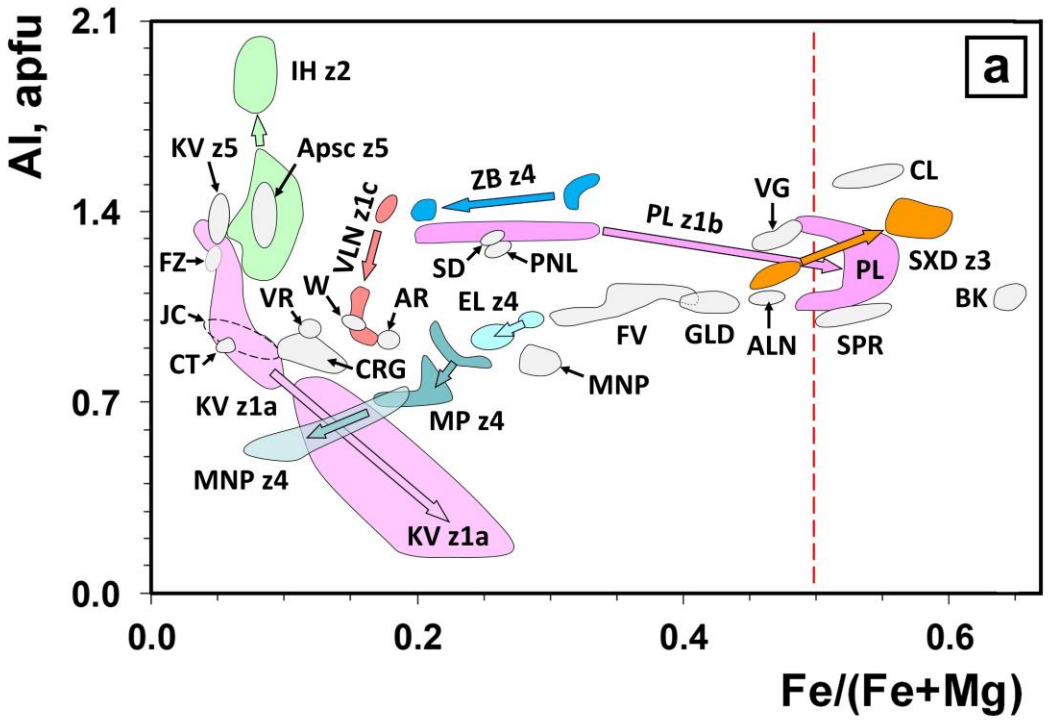

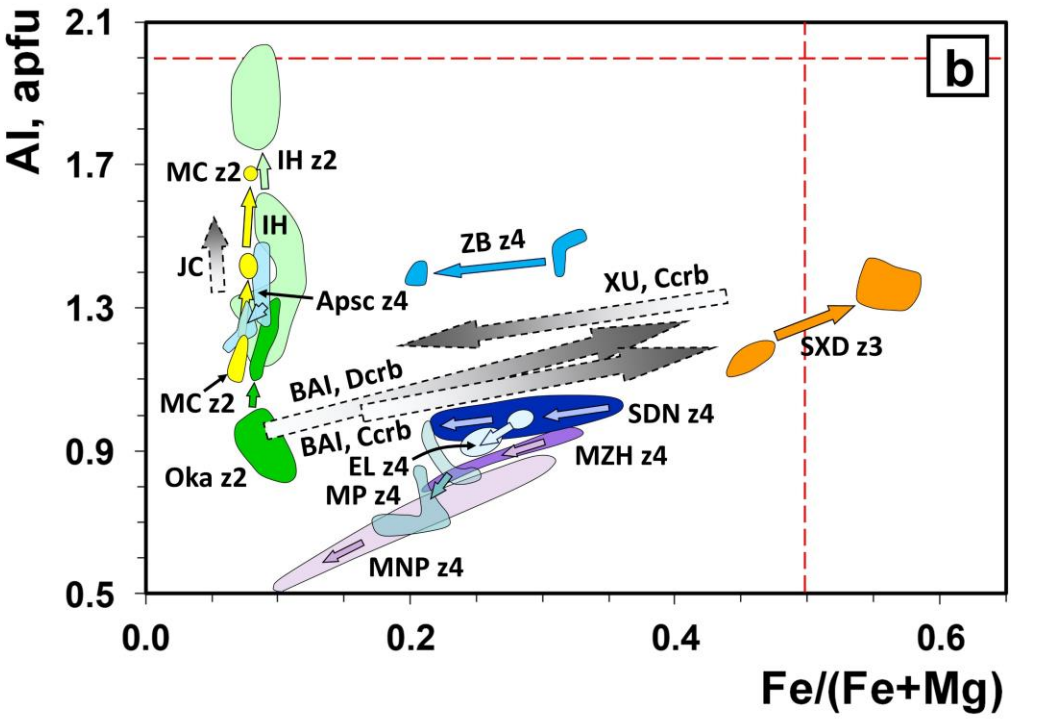

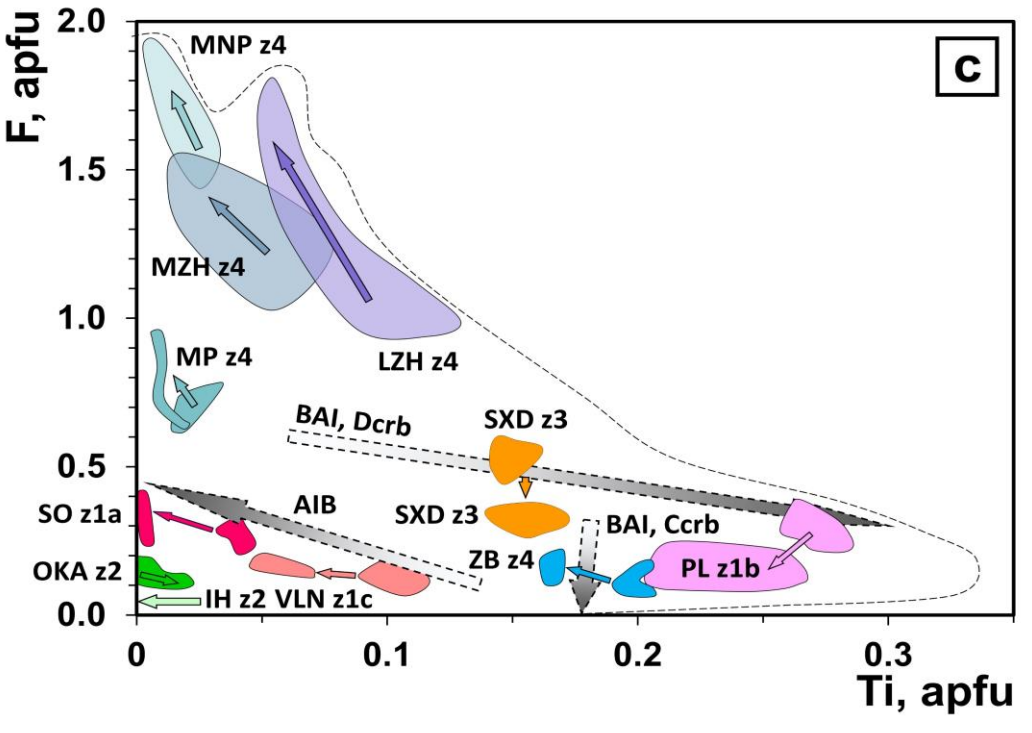

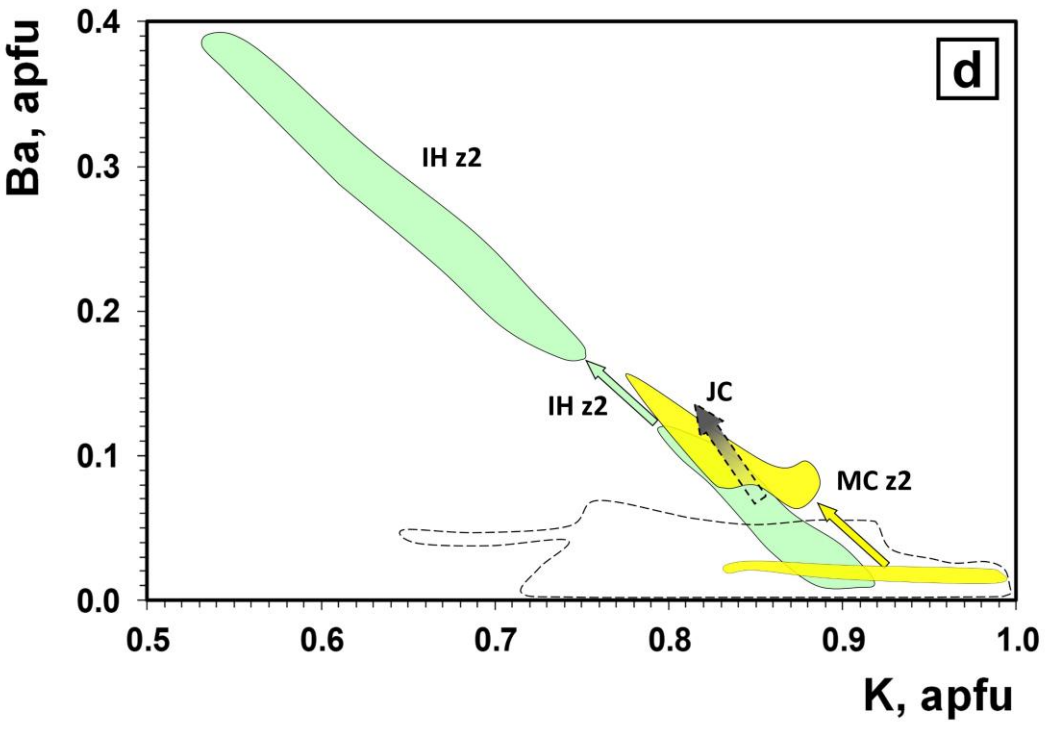

Fig. 5
Chakhmouradian et al., *Micas in carbonatites*

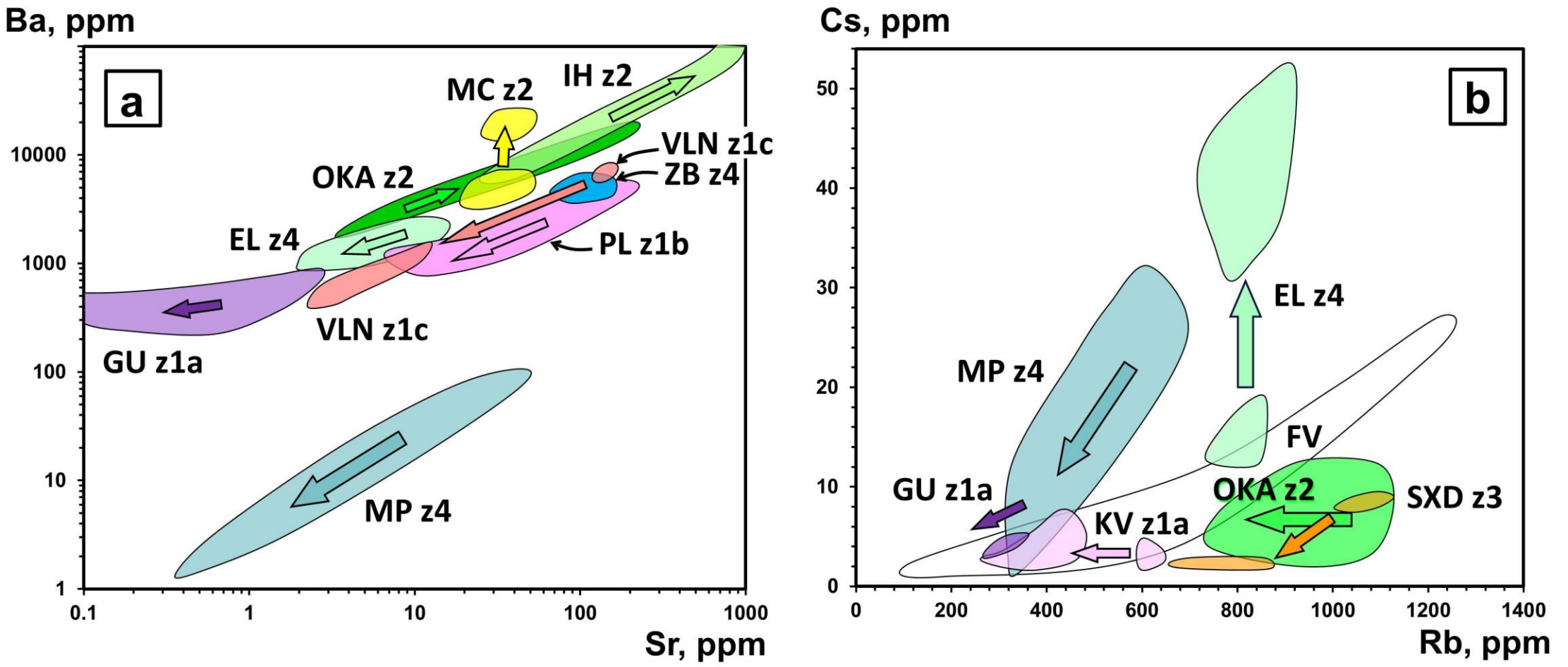

Fig. 6

Chakhmouradian et al., *Micas in carbonatites*

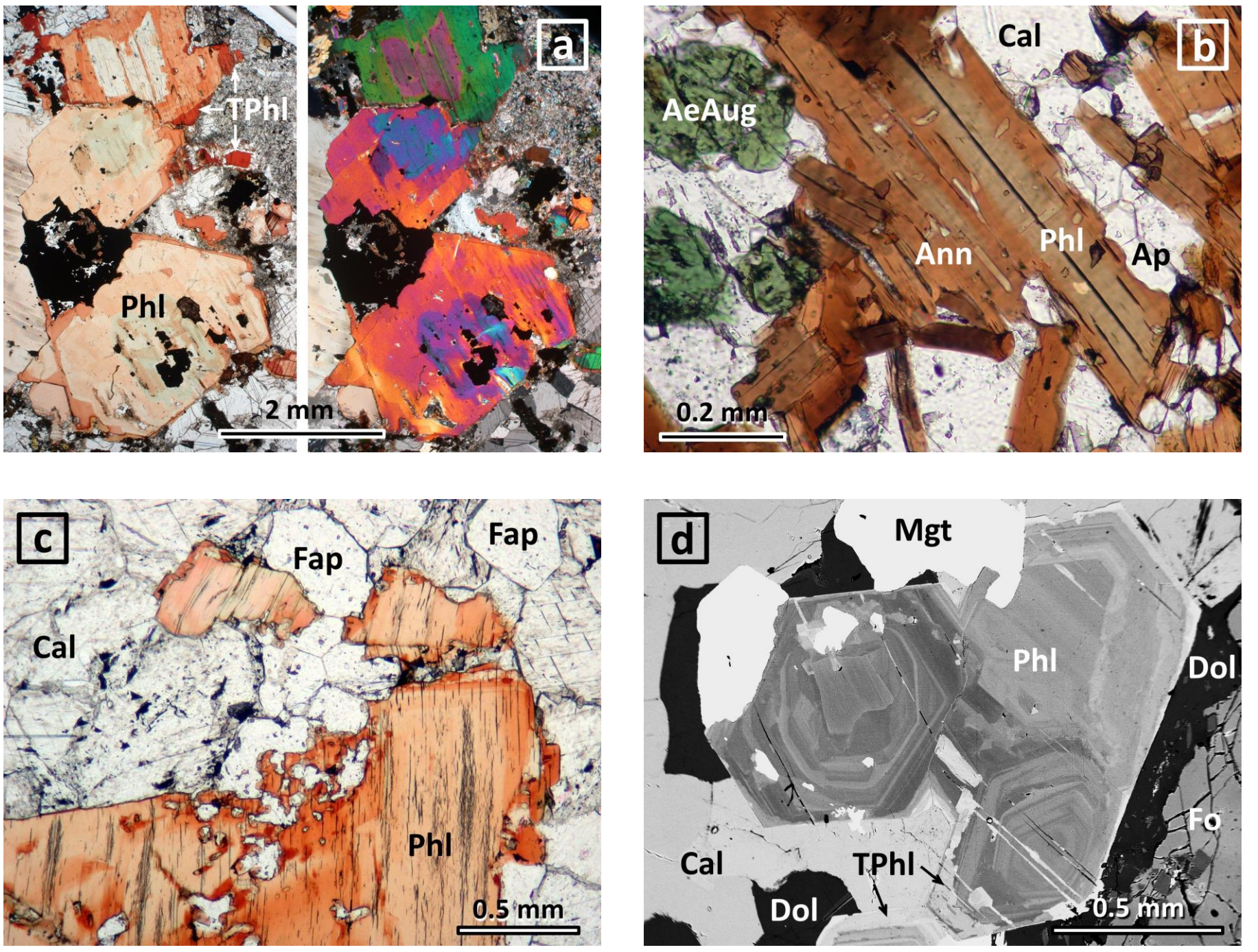

Fig. 7
Chakhmouradian et al., *Micas in carbonatites*

Supplementary Table 3. Selected major-element compositions of tainiolite and muscovite from carbonatite complexes.

	Dicker Willem[a]		Haast R.[a]	Chuktukon[b]	Cinder Lake			Fengzhen	Aley
Wt. %	crb	fen	fen	crb	after Kfs			after Pl	after Phl
Na_2O	0.40	0.72	n.d.	0.03	0.16	0.28	0.19	0.07	0.09
K_2O	11.41	11.39	11.12	11.57	11.49	11.00	11.02	10.37	10.63
CaO	n.d.	n.d.	n.d.	n.d.	0.01	0.03	0.02	0.07	0.11
BaO	n.a.	n.a.	n.a.	n.d.	0.08	0.16	0.06	0.16	n.d.
Li_2O	3.06	3.65[c]	2.81	3.50	n.a.	n.a.	n.a.	n.a.	n.a.
MgO	20.38	19.89	19.89	19.66	0.28	0.36	1.00	2.60	2.19
FeO	0.43	0.20	0.27	0.99	-	-	-	-	-
Fe_2O_3	-	-	-	-	0.83	2.11	6.70	0.36	1.11
TiO_2	0.01	0.04	0.03	0.13	0.09	n.d.	0.21	n.d.	0.05
Al_2O_3	0.07	0.35	0.48	0.09	36.92	35.74	32.01	31.03	29.67
SiO_2	57.44	58.03	59.61	58.58	46.07	44.97	44.46	50.07	50.68
F	9.09	9.70	9.51	9.13	n.d.	n.d.	n.d.	n.d.	n.d.
Atoms per formula unit (calculated assuming stoichiometry on the basis of 11 atoms of oxygen)									
Na	0.053	0.095	-	0.004	0.021	0.037	0.025	0.009	0.012
K	1.003	0.988	0.959	1.002	0.969	0.945	0.954	0.876	0.902
Ca	-	-	-	-	0.001	0.002	0.001	0.005	0.008
Ba	-	-	-	-	0.002	0.004	0.002	0.004	-
Li	0.848	0.974	0.764	0.955	-	-	-	-	-
Mg	2.094	2.017	2.004	1.989	0.028	0.036	0.101	0.257	0.217
Fe^{2+}	0.025	0.012	0.015	0.056	-	-	-	-	-
Fe^{3+}	-	-	-	-	0.041	0.107	0.342	0.018	0.056
Ti	0.001	0.002	0.002	0.007	0.004	-	0.011	-	0.003
Al	0.006	0.028	0.038	0.007	2.876	2.835	2.560	2.422	2.326
Si	3.959	3.946	4.029	3.975	3.045	3.027	3.016	3.316	3.370
F	1.981	2.086	2.033	1.959	-	-	-	-	-

[a] Dicker Willem, Namibia and Haast River, New Zealand (Cooper et al., 1995).
[b] Chuktukon, Siberia (Sharygin, 2017).
[c] Calculated on the basis of stoichiometry.
crb = carbonatite; fen = fenite; Kfs = potassium feldspar; Phl = phlogopite; Pl = plagioclase; n.a. = not analyzed; n.d. = not detected.

Supplementary Table 4. Compositional (major-element) variations in DTM from carbonatites and phoscorites: phlogopite with Type-I zoning, tetra-ferriphlogopite and annite

	Kovdor (KV-226)				Guli				Sokli				Prairie Lake			
	core		rim		core		rim		core		rim		core		rim	
Wt. %	min	max	min	max	min	max	min	max	min	max	min	max	min	max	min	max
Na_2O	0.39	0.52	0.40	0.57	0.15	0.20	0.14	0.26	0.71	0.81	0.71	0.81	0.23	0.29	0.12	0.23
K_2O	8.06	10.29	8.10	10.06	10.54	10.74	10.10	10.23	8.67	9.39	9.10	9.86	9.63	9.89	8.79	9.70
CaO	0.01	0.07	0.02	0.08	0.02	0.06	0.02	0.06	n.d.	0.07	0.04	0.20	0.02	0.03	n.d.	0.62
BaO	n.d.	0.59	n.d.	0.2	n.d.	0.17	0.08	0.13	0.07	0.13	n.d.	0.04	0.60	0.80	0.12	0.67
MgO	25.36	28.11	24.70	27.93	25.15	26.13	24.83	25.54	24.94	26.42	25.18	26.76	15.33	18.85	9.84	11.86
MnO	n.d.	0.08	0.03	0.10	0.06	0.09	0.20	0.29	0.03	0.11	0.03	0.13	0.07	0.29	0.49	0.63
FeO	n.d.	2.40	n.d.	16.42	3.21	4.75	2.88	3.74	3.51	5.15	2.32	4.53	8.84	14.11	19.77	25.01
Fe_2O_3	1.10	4.37	n.d.	13.26	0.08	5.07	12.40	14.01	0.52	2.83	4.44	10.20	n.d.	n.d.	n.d.	n.d.
Al_2O_3	10.25	16.04	1.79	9.10	7.39	10.61	1.06	2.49	11.34	12.22	4.54	9.03	14.33	15.09	11.09	14.48
SiO_2	38.65	43.02	39.01	43.17	40.47	41.83	39.82	40.28	40.86	41.70	40.85	42.43	33.49	36.31	32.66	36.78
TiO_2	0.12	0.35	0.03	0.42	0.02	0.28	n.d.	0.04	0.64	0.87	0.03	0.10	4.70	5.03	3.46	4.48
F	0.51	0.93	0.13	0.68	1.37	2.20	0.97	1.33	0.94	0.38	1.00	1.79	0.089	1.46	0.36	0.86
Cl	n.d.	n.d.	n.d.	n.d.	n.d.	n.d.	n.d.	n.d.	n.d.	n.d.	n.d.	n.d.	n.d.	n.d.	n.d.	n.d.
Atoms per formula unit (calculated assuming stoichiometry on the basis of 11 atoms of oxygen)																
Na	0.054	0.072	0.057	0.080	0.021	0.029	0.021	0.038	0.128	0.177	0.099	0.115	0.033	0.042	0.018	0.036
K	0.725	0.954	0.749	0.939	0.981	1.000	0.976	0.980	0.791	0.854	0.838	0.898	0.909	0.965	0.888	0.994
Ca	0.001	0.005	0.002	0.015	0.002	0.005	0.002	0.005	-	0.005	0.003	0.016	0.002	0.003	-	0.053
Ba	-	0.016	-	0.001	-	0.005	0.002	0.004	0.002	0.004	-	0.001	0.017	0.023	0.004	0.021
Mg	2.734	2.935	2.758	3.143	2.772	2.836	2.803	2.859	2.653	2.807	2.770	2.851	1.781	2.087	1.171	1.390
Mn	-	0.005	-	0.006	0.004	0.006	0.013	0.019	0.002	0.007	0.002	0.008	0.004	0.019	0.033	0.043
Fe^{2+}	-	0.143	-	0.257	0.195	0.294	0.181	0.237	0.097	0.305	0.139	0.280	0.549	0.919	1.295	1.576
Fe^{3+}	0.059	0.230	0.274	0.863	0.004	0.284	0.701	0.798	0.028	0.152	0.240	0.654	-	-	-	-
Al	0.846	1.333	0.153	0.781	0.640	0.906	0.095	0.220	0.950	1.019	0.393	0.760	1.298	1.334	1.030	1.341
Si	2.750	3.014	2.863	3.126	3.007	3.039	3.017	3.049	2.912	2.958	2.989	3.040	2.609	2.692	2.651	2.878
Ti	0.006	0.019	0.002	0.023	0.001	0.016	n.d.	0.002	0.034	0.047	0.001	0.006	0.262	0.284	0.208	0.265
F	0.113	0.207	0.031	0.217	0.320	0.505	0.232	0.319	0.212	0.307	0.233	0.406	0.219	0.343	0.091	0.214
Cl	-	-	-	-	-	-	-	-	-	-	-	-	-	-	-	-
Fe#	0.041	0.100	0.094	0.272	0.082	0.153	0.236	0.270	0.081	0.117	0.126	0.223	0.208	0.340	0.494	0.565
ΔT	-0.101	0.173	0.246	0.862	0.064	0.337	0.757	0.856	0.050	0.100	0.251	0.587	0.005	0.073	0.003	0.145

Fe# = $Fe_\Sigma/(Fe_\Sigma + Mg)$; tetrahedral site deficiency $\Delta T = 4 - (Si + Al)$; n.d. = not detected.

Supplementary Table 4. (continued).

	Aley cumulate				Valentine				Aley carb.		Kovdor (KV-26)		Cinder Lake
	core		rim		core		rim						
Wt. %	min	max	min	max	min	max	min	max	min	max	min	max	annite
Na_2O	0.05	0.43	0.03	0.07	0.45	0.63	0.48	0.61	0.17	0.47	0.89	1.08	0.04
K_2O	8.91	10.05	8.95	9.89	9.48	9.77	9.70	10.00	9.46	10.24	8.71	9.67	9.92
CaO	n.d.	0.06	0.01	0.07	n.d.	n.d.	n.d.	0.01	0.01	0.16	n.d.	0.22	n.d.
BaO	n.d.	0.10	n.d.	0.09	0.78	0.93	0.03	0.18	n.d.	n.d.	n.d.	0.06	n.d.
MgO	24.41	26.76	22.92	25.55	20.61	21.29	22.97	23.76	23.48	25.38	26.28	26.90	9.55
MnO	0.05	0.10	0.03	0.09	0.09	0.12	0.05	0.11	0.01	0.14	n.d.	0.07	0.14
FeO	0.38	4.23	3.22	8.37	9.70	9.16	7.66	8.36	4.08	7.94	2.03	3.23	21.27
Fe_2O_3	3.71	13.14	7.35	10.58	n.d.	n.d.	n.d.	0.48	2.46	4.63	5.97	9.85	-
Al_2O_3	5.52	7.79	5.39	6.01	16.25	16.62	11.03	12.90	5.95	9.52	4.89	8.06	16.91
SiO_2	39.79	42.77	41.84	43.23	37.37	37.79	40.00	41.65	41.45	42.78	41.28	42.09	34.97
TiO_2	0.01	0.09	0.01	0.16	1.71	2.11	0.90	1.28	0.06	0.29	0.05	0.18	2.00
F	3.52	4.18	3.02	3.73	0.32	0.76	0.59	0.79	2.94	4.26	0.25	0.35	0.70
Cl	n.d.	0.03	n.d.	n.d.	n.d.	n.d.	n.d.	n.d.	n.d.	n.d.	n.d.	n.d.	n.d.
Atoms per formula unit (calculated assuming stoichiometry on the basis of 11 atoms of oxygen)													
Na	0.007	0.062	0.004	0.010	0.063	0.088	0.067	0.085	0.024	0.067	0.123	0.150	0.007
K	0.857	0.921	0.826	0.931	0.874	0.899	0.884	0.919	0.890	0.963	0.810	0.892	0.985
Ca	-	0.005	0.001	0.005	-	-	-	-	-	0.012	-	0.017	-
Ba	-	0.003	-	0.003	0.022	0.026	0.001	0.005	-	-	-	0.002	-
Mg	2.716	2.866	2.472	2.730	2.222	2.287	2.469	2.533	2.581	2.736	2.838	2.880	1.108
Mn	0.003	0.006	0.002	0.006	0.005	0.007	0.003	0.007	0.001	0.008	-	0.004	0.009
Fe^{2+}	0.023	0.254	0.193	0.506	0.500	0.508	0.461	0.504	0.246	0.489	0.123	0.196	1.384
Fe^{3+}	0.201	0.729	0.336	0.570	-	-	-	0.026	0.135	0.258	0.325	0.539	-
Al	0.480	0.660	0.462	0.512	1.380	1.417	0.936	1.096	0.516	0.816	0.420	0.680	1.551
Si	2.955	3.073	3.033	3.127	2.703	2.722	2.884	2.978	3.008	3.129	2.971	3.047	2.721
Ti	0.001	0.005	0.001	0.009	0.093	0.115	0.049	0.069	0.003	0.016	0.003	0.013	0.117
F	0.821	0.950	0.691	0.847	0.074	0.173	0.136	0.179	0.688	0.982	0.057	0.080	0.172
Cl	-	0.004	-	-	-	-	-	-	-	0.001	-	-	-
Fe#	0.139	0.211	0.219	0.263	0.180	0.186	0.159	0.170	0.140	0.210	0.139	0.196	0.555
ΔT	0.267	0.566	0.360	0.501	-0.102	-0.119	0.020	0.086	0.172	0.367	0.349	0.562	-0.272

Fe# = $Fe_\Sigma/(Fe_\Sigma + Mg)$; tetrahedral site deficiency $\Delta T = 4 - (Si + Al)$; n.d. = not detected.

Supplementary Table 5. Compositional (major-element) variations in DTM from carbonatites and phoscorites: Type-II zoning

	Iron Hill				Oka				Magnet Cove				Kovdor*	
	core		rim		core		rim		core		rim			
Wt. %	min	max	min	max	min	max	min	max	min	max	min	max	min	max
Na_2O	0.49	0.79	0.51	0.69	0.20	0.34	0.27	0.33	0.11	0.18	0.16	0.20	0.29	1.59
K_2O	8.66	10.00	5.54	7.92	10.08	10.39	9.6	10.11	9.96	10.73	8.20	9.60	8.40	10.83
CaO	0.01	0.07	0.01	0.09	n.d.	0.12	0.02	0.07	0.03	0.23	0.04	0.22	n.d.	0.06
BaO	0.48	3.96	6.00	12.72	0.26	0.78	1.05	1.79	0.51	0.69	2.41	5.08	0.19	2.35
MgO	23.13	25.59	21.60	22.95	25.6	26.57	23.87	25.24	25.46	25.68	22.72	25.15	25.09	26.77
MnO	0.16	0.30	0.11	0.23	0.68	1.01	0.62	0.75	0.13	0.21	0.14	0.21	n.d.	0.04
FeO	1.54	3.80	1.58	3.05	1.39	3.36	2.58	3.71	0.69	3.23	0.32	2.69	n.d.	1.06
Fe_2O_3	0.95	3.90	0.71	2.58	2.05	3.95	0.69	2.27	n.d.	2.94	0.97	3.91	1.18	2.14
Al_2O_3	13.76	18.79	20.38	22.32	9.85	11.89	13.17	15.48	13.05	14.51	16.25	19.05	15.23	19.30
SiO_2	34.83	40.01	29.22	33.70	40.87	42.00	37.36	40.13	39.75	41.10	34.01	37.83	36.51	39.70
TiO_2	n.d.	0.56	n.d.	n.d.	n.d.	0.16	0.15	0.40	0.03	0.17	n.d.	n.d.	n.d.	0.06
F	0.08	0.43	0.13	0.40	0.46	0.77	0.39	0.67	0.15	0.38	0.04	0.31	n.d.	0.14
Cl	n.d.	n.d.	n.d.	n.d.	n.d.	n.d.	n.d.	n.d.	n.d.	0.02	n.d.	0.05	n.d.	n.d.
Atoms per formula unit (calculated assuming stoichiometry on the basis of 11 atoms of oxygen)														
Na	0.068	0.111	0.074	0.099	0.028	0.048	0.038	0.046	0.015	0.025	0.022	0.028	0.039	0.219
K	0.802	0.916	0.540	0.750	0.920	0.957	0.886	0.926	0.903	0.991	0.784	0.884	0.761	0.983
Ca	0.001	0.005	0.001	0.007	-	0.009	0.002	0.005	0.002	0.018	0.003	0.014	-	0.004
Ba	0.014	0.113	0.175	0.381	0.007	0.022	0.030	0.051	0.014	0.019	0.068	0.149	0.005	0.065
Mg	2.520	2.737	2.467	2.539	2.743	2.840	2.590	2.703	2.719	2.803	2.540	2.686	2.662	2.834
Mn	0.010	0.018	0.007	0.015	0.041	0.062	0.038	0.046	0.008	0.013	0.009	0.013	-	0.002
Fe^{2+}	0.095	0.230	0.098	0.191	0.083	0.203	0.159	0.225	0.041	0.196	0.019	0.166	-	0.062
Fe^{3+}	0.053	0.217	0.040	0.146	0.110	0.212	0.038	0.126	-	0.156	0.054	0.211	0.063	0.115
Al	1.168	1.608	1.774	2.010	0.837	1.003	1.120	1.321	1.115	1.216	1.399	1.683	1.278	1.619
Si	2.575	2.847	2.250	2.489	2.922	3.002	2.747	2.885	2.826	2.912	2.550	2.719	2.598	2.783
Ti	-	0.030	-	-	-	0.009	0.008	0.022	0.002	0.009	-	-	-	0.003
F	0.018	0.096	0.031	0.096	0.104	0.174	0.089	0.152	0.033	0.085	0.009	0.070	-	0.032
Cl	-	-	-	-	-	-	-	-	-	0.002	-	0.006	-	-
Fe#	0.068	0.115	0.071	0.097	0.072	0.111	0.082	0.099	0.065	0.076	0.075	0.083	0.039	0.053
ΔT	-0.218	0.016	-0.286	-0.227	0.064	0.184	-0.072	0.006	-0.058	0.021	-0.233	-0.072	-0.217	-0.047

Fe# = $Fe_\Sigma/(Fe_\Sigma + Mg)$; tetrahedral site deficiency $\Delta T = 4 - (Si + Al)$; n.d. = not detected; * phoscorite #KV-4 (oscillatory zoning).

Supplementary Table 5 (continued).

	Fengzhen			
	core		rim	
Wt. %	min	max	min	max
Na_2O	0.49	0.79	0.51	0.69
K_2O	8.66	10.00	5.54	7.92
CaO	0.01	0.07	0.01	0.09
BaO	0.48	3.96	6.00	12.72
MgO	23.13	25.59	21.60	22.95
MnO	0.16	0.30	0.11	0.23
FeO	1.54	3.80	1.58	3.05
Fe_2O_3	0.95	3.90	0.71	2.58
Al_2O_3	13.76	18.79	20.38	22.32
SiO_2	34.83	40.01	29.22	33.70
TiO_2	n.d.	0.56	n.d.	n.d.
F	0.08	0.43	0.13	0.40
Cl	n.d.	n.d.	n.d.	n.d.
Atoms per formula unit				
Na	0.068	0.111	0.074	0.099
K	0.802	0.916	0.540	0.750
Ca	0.001	0.005	0.001	0.007
Ba	0.014	0.113	0.175	0.381
Mg	2.520	2.737	2.467	2.539
Mn	0.010	0.018	0.007	0.015
Fe^{2+}	0.095	0.230	0.098	0.191
Fe^{3+}	0.053	0.217	0.040	0.146
Al	1.168	1.608	1.774	2.010
Si	2.575	2.847	2.250	2.489
Ti	-	0.030	-	-
F	0.018	0.096	0.031	0.096
Cl	-	-	-	-
Fe#	0.068	0.115	0.071	0.097
ΔT	-0.218	0.016	-0.286	-0.227

Fe# = $Fe_\Sigma/(Fe_\Sigma + Mg)$; tetrahedral site deficiency $\Delta T = 4 - (Si + Al)$; n.d. = not detected.

Supplementary Table 6. Compositional (major-element) variations in DTM from carbonatites and phoscorites: phlogopite-annite with Type-III zoning (Shaxiongdong) and phlogopite with Type-IV zoning.

	Shaxiongdong				Zibo (phenocrysts)				Aley phoscorite			
	core		rim		core		rim		core		rim	
Wt. %	min	max	min	max	min	max	min	max	min	max	min	max
Na_2O	0.14	0.26	0.09	0.17	0.09	0.15	0.07	0.10	0.89	1.30	0.91	1.31
K_2O	9.86	10.12	9.82	10.06	9.67	10.02	10.01	10.34	7.67	9.02	8.31	8.65
CaO	n.d.	0.02	n.d.	0.08	0.01	0.08	0.02	0.05	n.d.	0.03	0.01	0.05
BaO	n.d.	n.d.	n.d.	n.d.	0.47	0.80	0.45	0.72	n.d.	n.d.	n.d.	n.d.
MgO	11.48	12.61	8.70	9.67	15.45	16.08	19.06	19.33	23.49	24.89	25.39	26.22
MnO	0.24	0.37	0.20	0.34	0.06	0.08	0.04	0.06	0.03	0.16	0.04	0.09
FeO	19.17	19.98	21.98	24.06	13.21	14.04	8.93	9.35	n.d.	2.17	n.d.	0.31
Fe_2O_3	n.d.	n.d.	n.d.	n.d.	n.d.	n.d.	n.d.	n.d.	2.35	4.73	3.43	4.37
Al_2O_3	12.58	13.37	14.38	15.76	16.15	17.13	15.99	16.38	15.04	17.07	14.42	15.66
SiO_2	38.18	38.88	35.40	37.00	35.22	36.20	36.64	37.36	36.11	38.74	38.90	39.73
TiO_2	2.57	2.81	2.45	2.93	3.48	3.70	3.00	3.09	n.d.	0.18	0.02	0.13
F	1.86	2.34	1.08	1.45	0.28	0.65	0.46	0.82	0.48	1.10	1.27	1.48
Cl	n.d.	0.03	n.d.	0.04	n.d.	0.04	n.d.	0.02	n.d.	0.02	n.d.	n.d.
Atoms per formula unit (calculated assuming stoichiometry on the basis of 11 atoms of oxygen)												
Na	0.020	0.038	0.014	0.025	0.013	0.022	0.010	0.014	0.124	0.185	0.125	0.181
K	0.954	0.978	0.974	0.987	0.920	0.951	0.935	0.966	0.719	0.835	0.754	0.787
Ca	-	0.002	-	0.006	0.001	0.006	0.002	0.004	-	0.002	0.001	0.004
Ba	-	-	-	-	0.014	0.023	0.013	0.021	-	-	-	-
Mg	1.295	1.426	1.010	1.104	1.708	1.779	2.080	2.100	2.575	2.674	2.691	2.780
Mn	0.015	0.024	0.013	0.022	0.004	0.005	0.002	0.004	0.002	0.010	0.002	0.005
Fe^{2+}	1.219	1.268	1.414	1.566	0.822	0.874	0.546	0.573	-	0.131	-	0.019
Fe^{3+}	-	-	-	-	-	-	-	-	0.127	0.261	0.184	0.233
Al	1.125	1.190	1.313	1.429	1.412	1.502	1.379	1.414	1.276	1.479	1.209	1.312
Si	2.897	2.940	2.755	2.833	2.621	2.685	2.684	2.725	2.674	2.813	2.765	2.825
Ti	0.146	0.161	0.143	0.171	0.194	0.206	0.164	0.170	-	0.010	0.001	0.007
F	0.445	0.561	0.262	0.354	0.066	0.152	0.106	0.189	0.109	0.252	0.286	0.333
Cl	-	0.004	-	0.006	-	0.005	-	0.002	-	0.002	-	-
Fe#	0.461	0.491	0.564	0.608	0.320	0.338	0.207	0.215	0.083	0.092	0.062	0.079
ΔT	-0.123	-0.050	-0.199	-0.122	-0.138	-0.097	-0.110	-0.095	-0.167	-0.057	-0.078	-0.034

Fe# = $Fe_\Sigma/(Fe_\Sigma + Mg)$; tetrahedral site deficiency $\Delta T = 4 - (Si + Al)$; n.d. = not detected.

Supplementary Table 6 (continued).

	Eden Lake				Mountain Pass			
	core		rim		core		rim	
Wt. %	min	max	min	max	min	max	min	max
Na_2O	0.10	0.19	0.08	0.15	0.01	0.07	n.d.	0.11
K_2O	9.95	10.09	9.73	10.22	10.14	10.46	9.87	10.36
CaO	n.d.	0.01	n.d.	0.06	0.03	0.12	0.08	0.17
BaO	0.09	0.32	0.02	0.30	0.01	0.14	n.d.	0.11
MgO	17.94	18.35	18.71	19.33	20.93	21.55	21.19	23.08
MnO	0.27	0.30	0.25	0.29	0.06	0.09	0.06	0.09
FeO	13.08	13.68	11.46	12.54	9.86	11.92	8.98	11.28
Fe_2O_3	n.d.	n.d.	n.d.	n.d.	n.d.	1.07	n.d.	n.d.
Al_2O_3	11.22	11.44	10.47	11.02	9.59	11.13	8.12	9.77
SiO_2	40.50	40.97	41.66	42.56	40.39	41.74	41.77	44.59
TiO_2	0.70	0.84	0.52	0.73	0.31	0.60	0.18	0.37
F	3.00	3.77	3.45	4.10	2.67	3.23	2.72	4.10
Cl	0.01	0.10	n.d.	0.20	n.d.	0.03	0.01	0.01
Atoms per formula unit (calculated assuming stoichiometry on the basis of 11 atoms of oxygen)								
Na	0.014	0.027	0.011	0.021	0.001	0.010	-	0.015
K	0.941	0.960	0.916	0.962	0.955	0.982	0.908	0.962
Ca	-	0.001	-	0.005	0.002	0.009	0.006	0.013
Ba	0.003	0.009	0.001	0.009	-	0.004	-	0.003
Mg	2.006	2.035	2.066	2.125	2.304	2.367	2.299	2.481
Mn	0.017	0.019	0.016	0.018	0.004	0.006	0.004	0.005
Fe^{2+}	0.815	0.850	0.708	0.773	0.607	0.736	0.541	0.686
Fe^{3+}	-	-	-	-	-	0.059	-	-
Al	0.985	1.002	0.907	0.957	0.835	0.966	0.698	0.851
Si	3.016	3.049	3.070	3.127	2.975	3.070	3.085	3.214
Ti	0.039	0.047	0.029	0.040	0.017	0.033	0.010	0.021
F	0.706	0.884	0.808	0.950	0.621	0.754	0.635	0.935
Cl	0.001	0.013	-	0.025	-	0.004	0.001	0.001
Fe#	0.287	0.296	0.250	0.272	0.219	0.256	0.179	0.230
ΔT	-0.039	-0.014	-0.040	-0.026	0.035	0.137	0.064	0.088

Fe# = $Fe_\Sigma/(Fe_\Sigma + Mg)$; tetrahedral site deficiency $\Delta T = 4 - (Si + Al)$; n.d. = not detected.

Supplementary Table 7. Compositional (major-element) variations in sector-zoned phlogopite from carbonatites and phoscorites.

	Aley (PH1C)				Kovdor (KV-2)				Kovdor (KV-5)			
	high-AZ basal sector		low-AZ [001] zone sector		high-AZ basal sector		low-AZ [001] zone sector		high-AZ basal sector		low-AZ [001] zone sector	
Wt. %	min	max	min	max	min	max	min	max	min	max	min	max
Na_2O	0.93	1.30	0.89	1.22	0.98	1.53	0.64	1.31	0.80	2.38	0.75	1.92
K_2O	7.67	8.55	8.19	9.08	8.62	9.28	9.41	10.10	7.28	9.71	7.82	10.17
CaO	n.d.	0.03	n.d.	0.03	n.d.	0.14	n.d.	0.12	n.d.	0.14	n.d.	0.15
BaO	n.d.	n.d.	n.d.	n.d.	1.19	1.85	0.07	0.99	0.74	1.62	0.75	1.19
MgO	23.49	24.33	23.99	24.89	24.85	25.73	25.33	27.09	25.83	26.47	25.99	26.47
MnO	0.05	0.16	0.03	0.15	n.d.	0.03	n.d.	0.05	n.d.	0.04	n.d.	0.04
FeO	0.04	0.86	n.d.	2.17	0.72	2.44	0.75	2.67	0.29	1.32	n.d.	2.15
Fe_2O_3	3.69	4.73	2.35	4.73	1.09	2.35	0.76	2.09	0.96	2.58	0.62	2.86
Al_2O_3	16.61	17.07	15.04	16.65	16.85	17.33	11.44	16.77	15.55	16.74	15.54	16.22
SiO_2	36.11	37.99	36.80	39.01	37.26	38.72	38.26	42.07	38.18	39.54	38.79	39.61
TiO_2	n.d.	0.11	n.d.	0.18	0.07	0.20	0.03	0.14	0.02	0.11	0.03	0.07
F	0.48	0.99	0.63	1.10	0.30	0.38	0.28	0.55	0.13	0.28	0.13	0.25
Cl	n.d.	n.d.	n.d.	0.02	n.d.	n.d.	n.d.	n.d.	n.d.	n.d.	n.d.	n.d.
Atoms per formula unit (calculated assuming stoichiometry on the basis of 11 atoms of oxygen)												
Na	0.131	0.185	0.124	0.171	0.135	0.209	0.088	0.179	0.111	0.323	0.102	0.243
K	0.719	0.793	0.764	0.835	0.775	0.847	0.849	0.910	0.651	0.877	0.742	0.917
Ca	-	0.002	-	0.002	-	0.011	0.002	0.007	-	0.011	-	0.012
Ba	-	-	-	-	0.033	0.052	0.002	0.028	0.036	0.045	0.021	0.025
Mg	2.575	2.618	2.596	2.674	2.637	2.717	2.692	2.855	2.710	2.787	2.727	2.790
Mn	0.003	0.010	0.002	0.009	-	0.002	-	0.003	-	0.002	-	0.002
Fe^{2+}	0.002	0.052	-	0.131	0.043	0.145	0.044	0.158	0.017	0.103	-	0.127
Fe^{3+}	0.202	0.261	0.127	0.259	0.058	0.127	0.040	0.111	0.051	0.138	0.033	0.152
Al	1.408	1.479	1.276	1.424	1.408	1.443	0.953	1.409	1.314	1.386	1.296	1.339
Si	2.674	2.725	2.680	2.813	2.665	2.722	2.728	2.973	2.723	2.765	2.742	2.786
Ti	-	0.006	-	0.010	0.004	0.011	0.002	0.007	0.003	0.006	0.002	0.004
F	0.109	0.230	0.143	0.252	0.066	0.084	0.064	0.122	0.30	0.063	0.028	0.055
Cl	-	-	-	0.002	-	-	-	-	-	-	-	-
Fe#	0.083	0.090	0.084	0.092	0.052	0.077	0.054	0.069	0.050	0.055	0.051	0.056
ΔT	-0.147	-0.057	-0.167	-0.133	-0.148	-0.107	-0.140	0.074	-0.130	-0.055	-0.108	-0.059

Fe# = $Fe_\Sigma/(Fe_\Sigma + Mg)$; tetrahedral site deficiency $\Delta T = 4 - (Si + Al)$; n.d. = not detected.